THE ADSORPTION AND REACTION OF FLUORINE ON THE Si(100) SURFACE

J.R. ENGSTROM, Mark M. NELSON and Thomas ENGEL

Department of Chemistry, BG-10, University of Washington, Seattle, WA 98195, USA

The adsorption and reaction of both molecular and atomic fluorine with the Si(100) surface has been examined under ultrahigh vacuum conditions with supersonic molecular beam techniques, X-ray photoelectron spectroscopy (XPS), quadrupole mass spectrometry and low-energy ion scattering spectroscopy. Molecular fluorine adsorbs dissociatively on the clean Si(100) surface with an initial (zero-coverage) probability of adsorption of 0.46 ± 0.02, which is essentially independent of both the incident beam energy ($\langle E_{tr} \rangle = 1.5$–19 kcal mol^{-1}) and surface temperature ($T_s = 120$–600 K). The coverage-exposure relationship for F_2 is characterized by an initial rapid phase of adsorption, which saturates at a coverage of $\theta_F \simeq 1.5$ monolayers (ML), followed by a much slower phase of adsorption, which does not saturate even at an exposure of 600 ML. For substrate temperatures of 300 K and above, the rapid phase of adsorption is described well by second-order Langmuir kinetics. However, below 300 K, trapping into a mobile (molecular) extrinsic precursor state on the chemisorbed adlayer becomes important, which results in an adsorption probability that is nearly independent of coverage at 120 K. The adsorption of atomic fluorine is qualitatively different from molecular fluorine. Although the initial probability of adsorption is quite similar, i.e., approximately 0.5 ± 0.3; the adsorption probability of atomic fluorine is only weakly dependent on coverage, decreasing only by a factor of two at a coverage of 3–4 ML. Temperature-programmed decomposition of silicon-fluoride adlayers, produced by exposing the clean Si(100) surface at 120 K to a beam of fluorine, yielded $SiF_2(g)$ and $SiF_4(g)$ as the only gas phase reaction products. The relative yield of these two gas phase reaction products depends strongly on the initial coverage of fluorine adatoms – below ~ 3 ML, $SiF_2(g)$ is the major reaction product, whereas above ~ 3 ML, the yield of $SiF_2(g)$ remains constant while that of $SiF_4(g)$ increases continuously. Above initial coverages of 2 ML, the thermal decomposition is terminated near 800 K by the removal of one monolayer of the silicon substrate in the form of $SiF_2(g)$. A detailed analysis of the decomposition for coverages below 3 ML revealed complex behavior, the kinetics depending sensitively on the initial coverage of fluorine adatoms. For example, for initial coverages of 1–1.3 ML, zero-order kinetics were found to apply as the coverage decreases from 1.0 to 0.3 ML. A qualitative assessment of the adlayer configuration following partial decomposition suggests that the thermal decomposition in the zero-order regime proceeds inhomogeneously, leaving separate domains where the *local* coverage of fluorine is either near saturation or zero. We suggest that the spatially inhomogeneous decomposition is a manifestation of preferential reactivity at surface defects such as atomic steps. Investigation of the steady-state reaction between $F_2(g)$ and the Si(100) substrate for temperatures of 650–1200 K shows conclusively that fluorine must be adsorbed dissociatively for the gasification reaction [production of $SiF_2(g)$] to occur, i.e., a Langmuir–Hinshelwood mechanism dominates.

1. Introduction

The interaction of fluorine with silicon has attracted particular interest due to its fundamental role in the processing of microelectronic devices [1–29]. For example, fluorocarbon (e.g., CF_4) plasmas are commonly employed to etch silicon surfaces for pattern transfer [1,2]. In this case, the dominant reactive species in the plasma is generally believed to be fluorine atoms. Considerable technological interest exists also in the use of WF_6 in vapor phase deposition of thin tungsten metal films [3]. In the absence of hydrogen, this latter process results also in removal of Si substrate atoms, primarily in the form of SiF_4. In regards to a more fundamental point of view, most work to date that has examined the interaction of fluorine with surfaces of silicon has employed either XeF_2 [4–18], or fluorocarbon [19–21] or fluorine [22,23] radicals and /or ions as the gas phase source of fluorine. In particular, surprisingly little effort has been directed towards an examination of *molecular* fluorine with surfaces of silicon [24–26]. This may be due to the fact that molecular fluorine is thought to interact "weakly" with silicon surfaces, i.e., exposure of F_2 does not lead to an appreciable rate of "spontaneous etching" of the surface at room temperature [4,25], which does occur if silicon is exposed to XeF_2 [4]. Since similar reaction intermediates (e.g., SiF_x species, where $1 \leq x \leq 3$) can be expected to form from similar concentrations of fluorine adatoms, independent of the particular source of fluorine, an explanation for this observed difference between F_2 and XeF_2 or F atoms most probably involves the relative reactivity (i.e., the adsorption probability) of these gas phase species with both clean and partially fluorinated silicon surfaces [4,16]. Obviously, a detailed examination of the adsorption kinetics of F_2 on silicon would lend considerable insight into resolving these observations.

Winters and Coburn [4] have demonstrated that exposure of silicon to XeF_2 at room temperature results in an isotropic etching of the silicon surface, the rate being linear with the partial pressure of XeF_2 over a wide range of pressures, i.e., between approximately 4×10^{-4} and 1.4×10^{-2} Torr. Thus, under these reaction conditions, the etching rate was limited by the incident flux of XeF_2. The dominant gas phase reaction product was identified as SiF_4 [6]. More recent work has implicated both SiF and SiF_2 as minor gas phase reaction products [8]. SiF_2 has also been identified as a gas phase reaction product from the reaction of both fluorine atoms [23] and molecular fluorine [26] with surfaces of silicon. In regards to the reaction of XeF_2, McFeely and co-workers [17], employing soft X-ray photoelectron spectroscopy (XPS), have shown that the room temperature etching of silicon is dependent upon the buildup of a "thick" fluorosilyl layer, which involves approximately 6–7 monolayers (ML) of the silicon substrate. The dominant fluorine-containing species in this layer is SiF_3 [17].

McFeely and co-workers have also examined the distribution of adsorbed species on silicon surfaces resulting from relatively low exposures of XeF_2, employing both XPS [10] and electron energy loss spectroscopy (EELS) [11]. For fluorine concentrations corresponding to ~ 2 monolayers, SiF was found to be the dominant species on both the $(100) - (2 \times 1)$ and $(111) - (2 \times 1)$ surfaces of silicon. However, on the less "perfect" stepped, sputtered or (7×7) Si(111) surfaces, the relative abundance of the more highly fluorinated SiF_2 and SiF_3 species was found to be greater. Thus, it was suggested that, at low coverages, the SiF_2 and SiF_3 species are associated with defect sites such as atomic steps. Unlike the relatively thick fluorosilyl adlayers formed from high exposures of XeF_2, the adlayers corresponding to the monolayer regime have been found to be stable to substrate temperatures near 800 K [5,14]. Steinfeld and co-workers [14] have reported that SiF_4, SiF_2 and SiF are the only gas phase reaction products resulting from the thermal decomposition of fluorosilyl adlayers produced by exposure of silicon to XeF_2.

To the best of our knowledge, Stinespring et al. [24] have conducted the only relatively detailed examination of the adsorption kinetics of both molecular and atomic fluorine on a silicon surface. Employing XPS and an effusive beam as the source of molecular fluorine, these investigators reported an initial probability of (dissociative) adsorption of F_2 on Si(111) at room temperature of ~ 0.7, and a "saturation" coverage of 6.5×10^{14} atoms cm^{-2}. For a beam of atomic fluorine, these same investigators reported a value for the initial probability of adsorption of F that was similar to that found for F_2, whereas considerably higher coverages could be obtained for comparable exposures of F versus F_2, e.g., the "saturation" coverage for atomic fluorine, although not explicitly assigned, was certainly in excess of 2×10^{15} atoms cm^{-2}. These experimental observations suggest that the crucial difference between F_2 and XeF_2 or F atoms in regard to the etching of silicon at room temperature lies in the relative probabilities of adsorption on a *partially fluorinated* silicon surface.

We have investigated in detail the interaction of fluorine with the Si(100) surface by employing supersonic molecular beam techniques, XPS, low-energy ion scattering spectroscopy (ISS) [30], and quadrupole mass spectrometry. Supersonic molecular beam techniques have proven to be most useful in the investigation of elementary gas–surface reactions [31,32]. In particular, molecular beam techniques permit a decoupling of the energy states of the incident gas phase molecules (e.g., the incident translational energy), and the energy states of the solid surface (e.g., the substrate temperature). In regards to the dissociative adsorption of diatomic molecules on solid surfaces, of obvious importance here, a number of investigators [33,34] have demonstrated that activation barriers to adsorption can be overcome by gas phase molecules possessing sufficient incident translational energy. Recent work has also demonstrated the importance of the internal energy states of the incident gas

phase molecules [35,36]. Finally, substrate temperature can be critical in regards to the ability of a surface mediate dissociative adsorption through a "precursor" state [37].

We shall report here a detailed study of the kinetics of the adsorption of molecular fluorine on a Si(100) surface. The effects of both the incident translational energy of the F_2 molecules, and the Si substrate temperature on the adsorption kinetics will be considered explicitly. For comparison, and in considerably less detail, we shall consider also the adsorption of atomic fluorine. In order to investigate the surface reactions that lead to the gasification of the Si substrate, the thermal decomposition of silicon-fluoride adlayers, produced by exposing the Si surface to a beam of F_2 (or a mixture of F_2 and F), will be considered in detail. Concerning this subject, a brief report has appeared previously [38]. Modulated molecular beam techniques [31] will be employed also to investigate the kinetics of the decomposition reaction, however, in this case emphasizing primarily the limit of very low coverages. Finally, the steady-state reaction of F_2 with the Si(100) surface will be examined as a function of the substrate temperature. Concerning this reaction, the effects of a coincident Ar^+ ion beam will also be considered. It is hoped that armed with knowledge of the independently derived adsorption and decomposition kinetics, a more complete understanding of the steady-state etching of Si by F_2 molecules will emerge.

2. Experimental procedures

2.1. Apparatus

The experiments described here were conducted in a turbomolecular-pumped stainless steel ultrahigh vacuum chamber, which has been described in detail previously [39]. Briefly, the main analysis chamber contains a sample, mounted on a manipulator, located at the foci of a hemispherical energy analyzer (Leybold-Heraeus EA-11/100), a dual anode X-ray source, a doubly-differentially-pumped scanning ion gun (Leybold-Heraeus IQE 12/38), and the molecular beam. The ionization source of the quadrupole mass spectrometer (UTI 100C, fitted with a Balzers cross-beam ionizer) is located 5.6 cm, line-of-sight, from the sample. Differential pumping of the mass spectrometer, important for experiments involving reactive scattering, is provided by a liquid nitrogen-cooled copper shroud with two collimating apertures, which surrounds the ionization region. For the specific system considered here, i.e. fluorine on silicon, line-of-sight differentially-pumped detection also minimizes spurious effects due to wall reactions, which may come into play since (highly reactive) radical species, such as SiF_2, are expected as reaction products [8,14,25,26]. Although this method of cryogenic differential

pumping was only marginally successful for SiF_4, high pumping speeds were effected for SiF_2. Because of inherent geometric limitations, a fixed sample geometry was employed in this study, with angles of $33°$, $75°$, and $59°$ between the sample normal and the energy analyzer, the molecular beam, and the mass spectrometer, respectively. All experiments were interfaced with an LSI 11/73 minicomputer, equipped with a home-built multichannel scaler that was employed for pulse-counting of both the mass spectrometer and energy analyzer signals. An 18-bit D/A converter was employed to program and/or multiplex either the mass spectrometer or the energy analyzer.

The molecular beam is formed from a variable temperature nozzle source located 57 cm from the sample. The nozzle assembly consists of a thin-walled Ni tube, sealed at one end, with a pin-hole orifice of diameter $\simeq 130$ μm spark-eroded in the side. The tube can be heated resistively and the temperature is measured with a chromel–alumel thermocouple spot-welded near the orifice. Prior to admission to the nozzle tube, the fluorine gas (either $10\%F_2$/Ar on $10\%F_2$/He, Matheson) was sent through a NaF "scrubber" to remove any HF impurity (i.e., via the reaction $NaF + HF \rightarrow NaHF_2$). The source chamber is pumped by a 20 000 $\ell\cdot s^{-1}$ diffusion pump, whereas the two intermediate beam forming chambers are pumped by 7000 $\ell\cdot s^{-1}$ diffusion pumps. The beam can be modulated just prior to entering the main analysis chamber, i.e., in the second intermediate chamber, by a 50% duty cycle rotating disk chopper at frequencies between 30 and 240 Hz. Modulation frequencies of less than 2 Hz can be obtained by employing a flag mounted in the source chamber between the nozzle and the skimmer. Finally, a pneumatically operated isolation valve separates the source chamber and the first intermediate chamber, providing accurate control of exposure times of the sample to the molecular beam.

The Si(100) crystals were cut from a wafer (p-type, 40–50 Ω cm) into 1×3 cm rectangles, subsequently treated with hot H_2SO_4, HF and NH_4OH/H_2O_2, and finally rinsed with distilled water before insertion into vacuum. The crystals were cleaned in situ by argon ion sputtering and annealing to 1170 K. Surface cleanliness was verified by XPS. The sample holder permits cooling of the crystal to 120 K by thermal contact with a reservoir of flowing liquid nitrogen, whereas heating of the crystal is provided by a combination of radiative (a tungsten filament mounted behind the crystal) and direct resistive heating (for Si, efficient at temperatures above 700–800 K). The crystal temperature is monitored by a chromel–alumel thermocouple spot-welded to a Ta clip attached to the edge of the crystal. Precise temperature control was effected by employing an optimal feedback control scheme, which utilizes the laboratory minicomputer as the control element [40]. Linear and step-function temperature profiles are obtained easily and reproducibly. A single routine was employed that enabled the minicomputer to control the temperature, and control (e.g., multiplex) and monitor either the mass spectrometer or the energy analyzer.

2.2. Measurement of absolute beam flux

The absolute flux of the molecular beam impinging on the sample was measured coincident with several experiments, i.e., primarily the XPS experiments examining the adsorption kinetics, by employing the following method. With the crystal removed from the path of the beam, the molecular beam is allowed to scatter in the main analysis chamber and the partial pressure rise of the reactant (i.e., beam) gas (ΔP_b) is monitored with the mass spectrometer. The mass spectrometer has been previously calibrated for absolute partial pressure measurements by employing an ion gauge and leaking a small amount of the reactant gas into the main chamber. Knowledge of the area of the beam that is intercepted by the sample (A_b) and the volumetric pumping speed of the reactant gas (S) in the main chamber permit a straightforward calculation of the beam flux F_b via $F_b = \Delta P_b S / k_B T_c A_b$, where k_B is Boltzmann's constant and T_c is the temperature of the chamber walls. The volumetric pumping speed is calculated by measuring the both pumping time constant (τ) and the volume (V_c) of the main chamber, i.e. $S = V_c / \tau$. The pumping time constant can be measured by modulating (chopping) the molecular beam at a number of frequencies and monitoring the resulting time-dependent partial pressure of the reactant gas with the mass spectrometer. Fourier analysis gives the frequency dependent amplitude response, $\Delta P_A(\omega) = \Delta P_A(0) / \sqrt{1 + (\omega \tau)^2}$, where ω is the radial frequency. Provided the radial frequency can be varied near $\omega \sim 1/\tau$, the pumping time constant can be measured accurately based on a fit $\Delta P_A(\omega)$ to ω employing the above equation.

The above outlined method for measurement of the absolute beam flux relies on the validity of a number of assumptions, which should be mentioned at this time. The method assumes that the pumping speed of the reactant gas is stable, the reactant gas is uniformily distributed in the main chamber, and the reactant gas is fully equilibrated with the chamber walls. Provided the reactant gas is both relatively unreactive with the chamber walls, and makes several collisions with the chamber walls before being pumped away, these assumptions will essentially be met. For the reactant gas we consider here, i.e., fluorine, these conditions are in general *not* met, due primarily to the high reactivity of this gas. Thus, a slightly different procedure was implemented. For the F_2/Ar gas mixtures, the above procedure was employed, except that the mass spectrometer signal for Ar was monitored. Due to the minimal mismatch in the masses of F_2(38 amu) and Ar (40 amu), we expect negligible "focusing" of the heavier component on the axis of the beam [41]. Consequently, we can compute the F_2 flux by measuring the Ar flux and relating the two by utilizing the relative concentrations at the stagnation conditions. For the F_2/He mixtures, the intensity of the F_2 signal ($m/e = 38$) scattered off the Si sample (at 120 K) and detected by the mass spectrometer was assumed to be proportional to the absolute beam flux. This signal was then compared to

the same signal obtained for a F_2/Ar mixture of known flux. Provided the scattered intensity is independent of the energy of incident F_2 molecules, this procedure permits an accurate estimate of the F_2 flux for the F_2/He mixtures.

2.3. Measurement of absolute coverages

Relative fluorine coverages were determined by XPS with a Mg $K\alpha$ source by computing the ratio of the integrated intensity of the F(1s) peak to that of the Si(2p) peak. Absolute coverages were obtained by comparing these F(1s)/Si(2p) intensity ratios to similar ones for the ratio, O(1s)/Si(2p), obtained for a known coverage of oxygen adatoms [39]. The relative sensitivity, F(1s)/O(1s), was accounted for by employing the known photoionization cross-sections [42] and the transmission function of the analyzer [43]. In a number of cases, the F(1s) feature was monitored in a time-resolved fashion at a single fixed energy. in these cases the electron energy analyzer was detuned purposely (200 eV pass energy) in order to minimize effects due to the shifts in either the peak position or shape with the coverage of fluorine adatoms [5]. Spot comparisons of peak heights and integrated areas for a range of coverages between 0.1 and 7 ML showed agreement within 5%. Drift in the XPS signals with either time or substrate temperature were found to be always less than 5% of the total signal.

Above coverages of one monolayer, corrections must be made for the attenuation of the F(1s) feature due to the (assumed) penetration of adsorbed fluorine atoms into the underlying substrate layers. To make this correction, one is forced to assume some configuration for the fluorosilyl adlayer. The simplest approach is to assume a "continuum" model for the adlayer, i.e., the fluorine adatoms are distributed uniformily (constant density of N_F) throughout an adlayer of some thickness δ [44]. Provided the inelastic mean free path (IMFP) of the F(1s) photoelectrons, $\lambda_{F(1s)}$, is known, the apparent (θ_a) and true (θ) coverages can be related via $\theta = -\theta_\infty \ln(1 - \theta_a/\theta_\infty)$, where $\theta_\infty = n_F \lambda_{F(1s)} \cos \Theta / n_s$ is the apparent coverage of an infinitely thick adlayer, $\lambda_{F(1s)} \cos \Theta$ is the escape depth, Θ is the angle between the surface normal and the detector, and n_s is the two-dimensional density equivalent to one monolayer (i.e., n_s/N_F is the "monolayer thickness"). Assuming a monolayer thickness of 1.36 Å (i.e., $N_F = 5.0 \times 10^{22}$ atoms cm^{-3} and $n_s = 6.8 \times 10^{14}$ atoms cm^{-2}), $\lambda_{F(1s)}$ can be estimated as 8.6 Å, which results in a value for θ_∞ of 5.3 ML [44]. This value for $\lambda_{F(1s)}$ is comparable to that employed previously by Gruntz et al. [28], where for Al $K\alpha$ radiation they assumed $\lambda_{F(1s)} = 13$ Å, which corresponds to ~ 11 Å for Mg $K\alpha$ radiation.

3. Results

3.1. Adsorption kinetics

3.1.1. Coverage dependence

The adsorption kinetics of F_2 on the Si(100) surface have been investigated by measuring the fluorine coverage via XPS (see section 2.3) as a function of exposure to a molecular beam of known flux (see section 2.2). A typical experiment would consist of annealing the crystal to 1170 K, cooling slowly to the desired temperature, verifying surface cleanliness with XPS, and exposing the crystal to the molecular beam by opening the isolation value that separates the source chamber from the first beam-forming chamber. After a specified period of time, the beam valve would be closed and XPS spectra would be collected in the F(1s) and Si(2p) regions. This procedure, i.e., exposing the crystal to the molecular beam for a specified time, followed by the XPS measurements, would be continued as desired. An alternate method was also employed that involved monitoring the F(1s) peak in real time at a single fixed energy (binding energy of $\simeq 686$ eV, energy analyzer pass energy of 200 eV) as the crystal was exposed to a constant flux of the molecular beam. Both the "sequential dose" and "continuous dose" methods each have their advantages. In particular, by dosing sequentially the X-ray source can be turned off during the gas exposure, which eliminates any artifacts due to the presence of high-energy photons, and the resulting integrated XPS spectra are not affected by shifts in the peak positions or shapes. By dosing continuously, a larger data set can be obtained more easily, contamination by background gases is reduced, and the exposure scale is more accurate since it is not the sum of individual, sequential exposures. In practice, we obtained similar results using either method.

Fluorine coverage is displayed as a function of F_2 exposure in fig. 1 for a single substrate temperature of 120 K. The data shown are for two beam gas mixtures of either 10%F_2 in Ar or 10%F_2 in He, and a nozzle temperature of 300 K, which correspond to average translational kinetic energies for the F_2 molecules of 1.48 and 8.0 kcal mol^{-1}, respectively [fluxes of $2.5 \times 10^{13}(F_2/Ar)$ and 1.1×10^{14} (F_2/He) molecules cm^{-2} s^{-1}]. Both the coverage and exposure are given in terms of monolayers (ML), where, for Si(100), 1 ML $\equiv 6.8 \times 10^{14}$ atoms cm^{-2}. In order to compare these data to others given in terms of langmuirs (L, 1 L $\equiv 10^{-6}$ Torr $\cdot$ s) for exposure units, 1 L of F_2 gas at 300 K is equal to 0.97 ML of F atoms. The coverages are given in both the apparent values, and the "corrected" values obtained by utilizing $\lambda_{F(1s)} = 8.6$ Å (i.e., $\theta_\infty = 5.3$ ML). Above ~ 2 ML, these "corrected" values should be viewed as *very* qualitative estimates (see section 2.3).

As may be seen in fig. 1, in both cases there is an initially rapid rate of adsorption, which saturates near a coverage of 1.5 ML, followed by a much
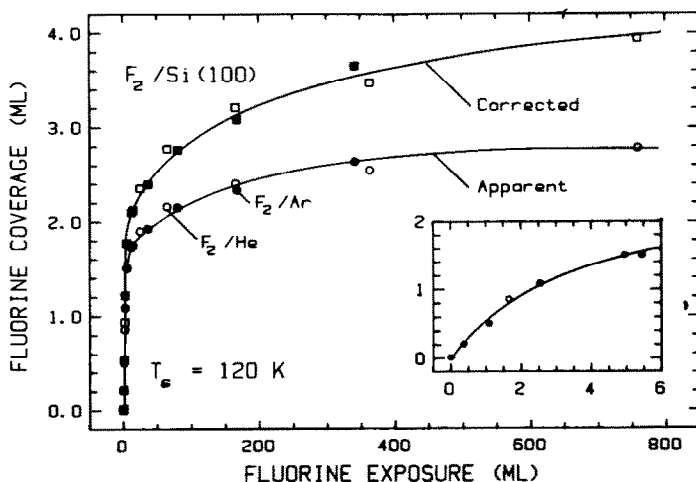
Fig. 1. The coverage–exposure relationship for the adsorption of F_2 on the clean Si(100) surface at a substrate temperature of 120 K. The filled symbols represent data obtained with a beam gas mixture of 10% F_2 in Ar ($\langle E_{tr} \rangle$ = 1.48 kcal mol^{-1}), and the open symbols a mixture of 10% F_2 in He ($\langle E_{tr} \rangle$ = 8.0 kcal mol^{-1}). The solid lines were drawn to aid the presentation. Both the apparent coverages (circles) and the "corrected" coverages (squares), for which the latter accounts for the attenuation of the F(1s) photoelectrons at high coverages (see text), are displayed. The initial rapid phase of adsorption is displayed in the inset. On the Si(100) surface, 1 ML $\equiv 6.8 \times 10^{14}$ atoms cm^{-2}.

slower rate of adsorption that apparently has not saturated at an exposure of 300–600 ML. The low exposure region, corresponding to the "rapid" phase of adsorption, has been replotted and is displayed in the insert in fig. 1. For the two cases shown, the average beam energy seems to have a negligible effect on either the initial probability or the coverage dependence for a surface temperature of 120 K. The break in the adsorption kinetics at a coverage near 1.5 ML is much more evident in the data displayed in fig. 2, which are representative of the low exposure regime, and correspond to four different substrate temperatures. All of the data displayed in fig. 2 were obtained with a 10%F_2 in Ar beam (flux of 4.5×10^{12} molecules cm^{-2} s^{-1}). At a substrate temperature of 120 K, the probability of adsorption (i.e., $d\theta/d\epsilon$, where ϵ is the exposure) is nearly independent of coverage up to ~ 1 ML. However, for substrate temperatures of 300 K and above, the probability of adsorption decreases rapidly with increasing coverage. Finally, although the four curves displayed in fig. 2 certainly differ at a finite coverage, the initial probability of adsorption on the clean Si(100) surface (S_{0,F_2}) appears to be relatively insensitive to the substrate temperature (see section 3.1.2 below). The insensitivity of S_{0,F_2} to the substrate temperature suggests that an *intrinsic* precursor [37,45] (i.e., a molecular adsorption state lying above an empty site) plays no role in
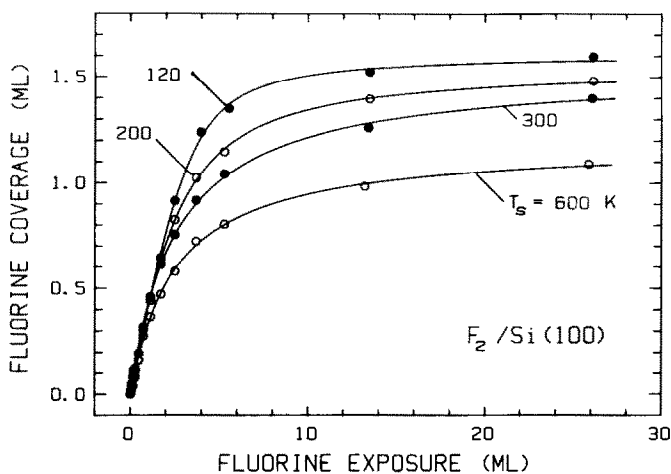
Fig. 2. The coverage–exposure relationship for the low exposure regime for F_2 on the clean Si(100) surface at four different substrate temperatures. In all cases, the beam gas mixture was 10% F_2 in Ar ($\langle E_{tr} \rangle = 1.48$ kcal mol^{-1}). The solid lines represent analytic fits of the adsorption kinetics to either a second-order Langmuir model [eq. (1); $T_s = 300$, 600 K)] or an extrinsic precursor model [eq. (2); $T_s = 120$, 200 K]. The experimental uncertainties are indicated by the size of the plotted symbols.

determining the adsorption kinetics. However, the weak dependence of the adsorption probability on coverage at a surface temperature of 120 K, and to a certain extent at 200 K, suggests that an *extrinsic* precursor (i.e., a molecular adsorption state lying above a filled site) is important at sufficiently low temperatures.

The coverage versus exposure curves for the low exposure regime shown in fig. 2 have been fit to a generalized form of Langmuirian kinetics given by

$$d\theta/d\epsilon \equiv S(\theta) = S_0(1 - \theta/\theta_s)^d,$$ (1)

where $S(\theta)$ is the probability of adsorption, θ_s is the "saturation" coverage and d is the "order". In general, all three of these quantities are functions of the substrate temperature. The order d was allowed to vary arbitrarily, and a nonlinear least-squares routine was used to find the optimal parameters. The data for substrate temperatures of 120 and 200 K are not fit well by this expression. On the other hand, for temperatures between 300 and 700 K, the data are described well by this model, with the optimal values for $d = 2.0 \pm 0.3$. Re-fitting the data by fixing $d = 2.0$ resulted in equally good agreement, i.e., within experimental uncertainties. The resulting fits for $d = 2.0$ and substrate temperatures of 300 and 600 K are shown in fig. 2. As may be seen, the agreement between the data and second-order Langmuir kinetics is excellent.

As pointed out above, the independence of the initial probability of adsorption on the substrate temperature (see section 3.1.2 below also) suggests that an intrinsic precursor is absent, whereas the weak dependence of the probability of adsorption on coverage at low surface temperatures (≤ 200 K) indicates that an extrinsic precursor is present. Cassuto and King [45] have derived an expression describing the probability of adsorption in cases for which an intrinsic precursor does not exist. If the trapping probability into the extrinsic precursor state (α') and the initial probability of (dissociative) adsorption into the chemisorbed state (S_0) are identical, this expression predicts that the adsorption probability will be independent of coverage at low coverages, i.e., exactly what we have observed here at $T_s = 120$ K. Consequently, the coverage versus exposure curves for $T_s \leq 300$ K were fit to this expression (where we assume $S_0 = \alpha'$), which is given by

$$S(\theta) = S_0(1 - \theta/\theta_s)^2 \left[1 + \frac{1 - (1 - \theta/\theta_s)^2}{K' + (1 - \theta/\theta_s)^2} \right], \tag{2}$$

where $K' = k_d'/k_m'$ is the ratio of the rate coefficient k_d' for desorption from the extrinsic precursor and the rate coefficient k_m' for migration from the extrinsic precursor to a vacant (nearest neighbor pair) adsite. Note that, based on the results at $T_s = 300$ and 600 K, in the absence of the extrinsic precursor, eq. (2) assumes second-order kinetics. For a "short-lived" extrinsic precursor, $K' \gg 1$, and eq. (2) gives (second-order) Langmuirian kinetics, i.e. eq. (1). For a "long-lived" precursor, $K' \ll 1$, and $S(\theta) \simeq \text{constant} = S_0$. The curves representing the optimal fits, obtained by employing a nonlinear least-squares procedure, are shown in fig. 2 for $T_s = 120$ and 200 K, where the optimal values were found to be $K' = 0.154$ and 1.06 respectively. As may be seen, for these two cases, the agreement between the model and the experimental data is excellent. As expected intuitively, the parameter K' was found to decrease with temperature (i.e., obviously, the activation energy E_d' must be greater than E_m'). The data for $T_s = 300$ K could also be fit by this model, with comparable uncertainty to that obtained with eq. (1), where for two separate experiments the mean optimal value was found to be 2.6. In practice, given our experimental uncertainties, for values of $K' \geq 3$, fits to eqs. (1) and (2) were found to be indistinguishable.

3.1.2. Initial probability of adsorption

The initial probability of adsorption S_0 was determined as a function of substrate temperature by evaluating the initial slope of coverage versus exposure curves, such as those displayed in fig. 2. These data are displayed in fig. 3. The independence of S_0 on the substrate temperature is readily apparent, where the mean value for $T_s = 120$–600 K was found to be 0.46 ± 0.02. As discussed above, this behavior suggests strongly that trapping into a molecular
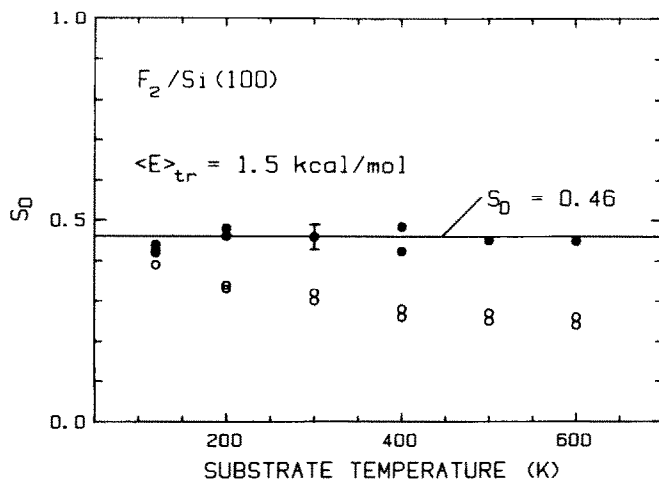
Fig. 3. The initial (zero-coverage) probability of dissociative adsorption of F_2 on the Si(100) surface as a function of substrate temperature. The solid circles were derived from the coverage–exposure relationships as determined from XPS, such as those displayed in fig. 2. The open circles were derived from the "beam reflectivity" method of King and Wells [46]. In all cases, the beam gas mixture was 10% F_2 in Ar ($\langle E_{tr} \rangle = 1.48$ kcal mol^{-1}).

precursor state lying above a vacant adsite is not a major pathway to dissociative chemisorption.

As a consistency check, an alternate technique, involving the "beam reflectivity" method proposed originally by King and Wells [46], was employed to measure the initial probability of adsorption. In the ideal case, this method permits a direct measurement of the probability of adsorption, independent of knowledge of either the beam flux or the absolute coverage. Basically, the method involves measurement of the decrease in the partial pressure of the reactant gas in the (continuously pumped) main analysis chamber caused by the "pumping" action of the crystal (i.e., that due to irreversible adsorption). If the crystal is exposed to the reactant via a molecular beam, as is the case here, the measurement is relatively straightforward [47]. However, the technique requires a stable pumping speed for the reactant gas. As discussed above in section 2.2, due to wall reactions, the pumping speed for F_2 can very significantly during the course of an experiment. Consequently, the mass spectrometer was employed to measure the direct reflected flux of F_2 at a single fixed angle with respect to the crystal. Although this minimizes effects due to varying pumping speeds, an additional complication arises if the angular distribution of the reflected flux is a function of the substrate temperature and/or adsorbate coverage.

The initial probabilities of adsorption determined via the "beam reflectivity" method are displayed also in fig. 3 as a function of the substrate

temperature. There is excellent agreement between these results and those obtained via XPS for $T_s = 120$ K. However, the apparent probability of adsorption determined by the "beam reflectivity" method clearly decreases with increasing substrate temperature. We suspect that this is an experimental artifact of the technique. In the particular, although the *absolute* accuracy of the XPS results is probably no better than $\pm 20\%$, the *internal* run-to-run consistency of the XPS results for different substrate temperatures is closer to 5%. Thus, the apparent decrease in S_0 with substrate temperature indicated by the "beam reflectivity" results is most probably a manifestation of an angular distribution of the reflected flux which is dependent upon the substrate temperature and/or adsorbate coverage.

The effect of average translational kinetic energy of the F_2 molecules on the initial probability of adsorption was investigated briefly. As displayed in the inset in fig. 1, for average translational energies of 1.48 and 8.0 kcal mol^{-1} and $T_s = 120$ K, the initial probabilities of adsorption are identical within experimental error. Essentially equivalent results were found for F_2 beams corresponding to average translational energies of 3.5 and 18.7 kcal mol^{-1}. Since $S_0 \simeq 0.5$, i.e., it is relatively near unity, even at a beam of 1.48 kcal mol^{-1}, the absence of any substantial increase in S_0 as the beam energy is increased to 19 kcal mol^{-1} is hardly surprising.

3.1.3. Atomic fluorine

The qualitative aspects of the adsorption kinetics of atomic fluorine on the Si(100) surface were investigated by thermally dissociating a fraction of the F_2 molecules in the beam to F atoms by heating the nozzle assembly to 965 K. This produces a beam in which 17% of F_2 molecules have been converted to F atoms (calculated value based on the measured stagnation F_2 partial pressure of 29 Torr). Due to the reactivity of fluorine and the thin-walled nature of our nozzle orifice, higher temperatures could not be used without the rapid degradation of the orifice [49].

Coverage versus exposure curves for two beams of differing average translational energies (4.8 and 26 kcal mol^{-1} for F_2, 2.4. and 13 kcal mol^{-1} for F) composed of a mixture of atomic and molecular fluorine are shown in fig. 4. Both the apparent coverages and "corrected" coverages, utilizing $\theta_\infty = 5.3$ ML, are displayed. The apparent coverages corresponding to beams of entirely molecular fluorine, given previously in fig. 1, are shown for comparison. Due primarily to the relatively low conversion to F atoms, we were unable to determine with high accuracy either the initial probability or the coverage dependence of adsorption of atomic fluorine. Concerning the initial probability of adsorption, an analysis gave a value of $S_{0,F} = 0.5 \pm 0.3$, i.e., it is on the same order as S_{0,F_2}. On the other hand, above coverages of approximately 1.5 ML, there is a definite difference in the adsorption kinetics between the F/F_2 and F_2 beams. In particular, on a partially fluorinated surface, the adsorption
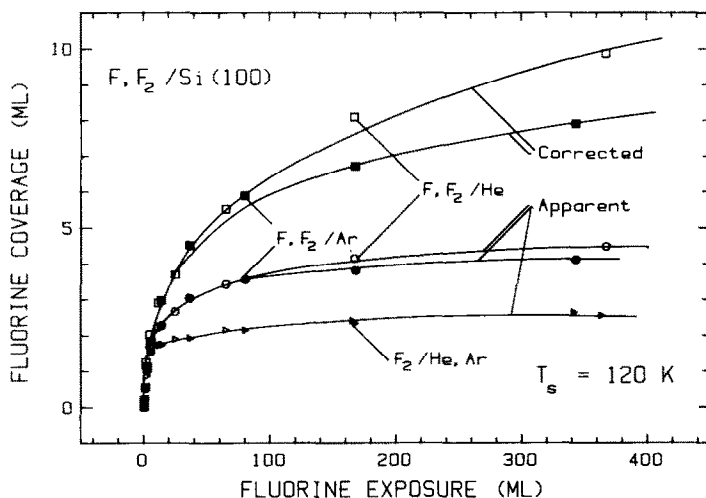
Fig. 4. The coverage–exposure relationships obtained for beams incident on a Si(100) surface that were composed of a mixture of atomic and molecular fluorine seeded in either Ar or He. The calculated fraction of molecular fluorine converted to atoms was 17%. The filled symbols represent data obtained with a beam gas mixture of 10% F_2 in Ar [$\langle E_{tr}\rangle = 4.8$ kcal mol^{-1} (F_2), 2.4 kcal mol^{-1} (F)], and the open symbols a mixture of 10% F_2 in He [$\langle E_{tr}\rangle = 26$ kcal mol^{-1} (F_2), 13 kcal mol^{-1} (F)]. The solid lines were drawn to aid the presentation. Both the apparent coverages (circles) and the "corrected" coverages (squares), for which the latter accounts for the attenuation of the F(1s) photoelectrons at high coverages (see text), are displayed. The apparent coverages for beams composed of entirely molecular fluorine (triangles), which are given above in fig. 1, are shown for comparison.

probability of F is much greater than that for F_2. For example, employing the corrected values for the coverages $S_{F_2} \simeq 1.2 \times 10^{-3}$ for $\theta_F \simeq 3$–4 ML, whereas the data shown in fig. 4 imply that $S_F \simeq 0.28$ for the same coverage range. The latter value was calculated based on the measured apparent probability of adsorption for the 10%F_2/He beam, $S_{app} = 0.048$, and employing the expression, $S_{app} = xS_F + (1-x)S_{F_2}$, where x is the fraction of F_2 in the beam converted to atoms. These observations, i.e., little difference between F_2 and F adsorption kinetics on a clean Si surface, whereas a significant difference on a partially fluorinated surface, are in agreement with those reported by Stinespring et al. [24].

Unlike the adsorption of molecular fluorine, the average translational energy does appear to exert some influence on the adsorption kinetics of atomic fluorine on a partially fluorinated surface. As may be seen in fig. 4, at a similar exposure and above coverages of 3–4 ML, the coverage obtained from the higher energy beam is greater than that obtained from the lower energy beam. This result implies that the adsorption of atomic fluorine on a partially

fluorinated surface, which most probably involves penetration into the Si lattice, is activated and can be overcome by translational energy.

3.1.4. Low-energy ion scattering measurements

Low-energy ion scattering spectroscopy (ISS) has been employed, in conjunction with XPS, in order to evaluate the extent of penetration of adsorbed fluorine atoms into the Si lattice and underlying sub-surface layers. For example, theoretical ab initio calculations have suggested that an "interstitial", near-surface form of adsorbed fluorine atoms should be stable on a Si substrate ("binding energy" of ~ 105 kcal mol^{-1}) [27]. ISS is extremely surface sensitive – the resulting spectra, which can provide compositional information, are representative of only the topmost layer [30]. XPS, on the other hand, as discussed above in section 2.3, is sensitive to fluorine located in 6–7 of the topmost layers of the Si substrate. Consequently, comparison of integrated XPS and ISS spectra as functions of either temperature or adsorbate coverage should reflect any qualitative changes in the near-surface distribution of fluorine adatoms.

The low-energy ion scattering spectra discussed here were obtained with 125 eV He$^+$ ions, this relatively low energy chosen in order to minimize sputtering of the adlayer. This is especially important for the fluorine–silicon system, since a number of investigators have shown that the presence of an ion beam can enhance the etching reaction between fluorine and silicon (i.e., via the so-called "chemical sputtering") [4,6,8,13,16]. Nevertheless, despite these precautions, sputtering was observed. In order to correct for this, three consecutive spectra were obtained and the resulting integrated areas were extrapolated to zero exposure of the ion beam. The IS spectra were obtained by exposing the Si(100) surface at 120 K to a molecular beam of F$_2$ ($\langle E_{tr} \rangle = 1.5$ kcal mol^{-1}). These spectra were found to be characterized by a sharp feature centered near 72 eV (FWHM = 7 eV), which was also present on the clean Si surface, and a rather broad feature centered near 48 eV (FWHM = 16 eV), which was present only after exposure to fluorine. These peak positions for Si and F are in good agreement with those predicted by the binary collision model [30], i.e., 75 and 50 eV, respectively.

The integrated Si and F ISS intensities are displayed in Fig. 5 as a function of the total fluorine adatom concentration as deduced by XPS. The substrate temperature in all cases was 120 K. There is a linear increase in the F signal and a concomitant decrease in the Si signal with increasing fluorine coverage. These results suggest that for these adsorbate concentrations and a substrate temperature of 120 K, the fluorine adatoms are confined to the topmost layer of the Si surface. This, of course, is not surprising if the initial "fast" adsorption phase of F$_2$ on Si(100) (i.e., up to ~ 1.5 ML) involves the attachment of fluorine adatoms to the Si dangling bonds present in the first substrate layer.
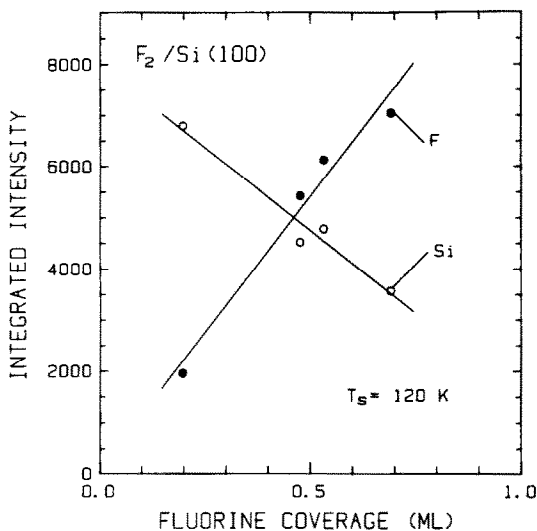
Fig. 5. Integrated intensities of the ISS peaks representative of Si and F as a function of the fluorine adatom coverage. The fluorine coverage was determined via XPS, and the substrate temperature in all cases was 120 K.

The effect of substrate temperature on the distribution of fluorine adatoms has also been investigated. These experiments involved adsorbing ~ 0.6 ML of fluorine on the Si(100) crystal at 120 K as described above, measuring the XP and IS spectra, annealing the sample to a higher temperature for ~ 100 s, and finally cooling to 120 K and measuring the XP and IS spectra again. In order to minimize deleterious effects due to sputtering, the ion beam was moved to a different location on the crystal before the second IS spectrum was taken. Although these experiments will obviously shed no light on the equilibrium distribution of fluorine adatoms, any irreversible penetration by fluorine should be detectable. An appropriate parameter to assess the extent of penetration is the ratio of the "after anneal" and "before anneal" values for quantity $(\int I_F \, dE / \int I_{Si} \, dE)/\theta_F$, where $\int I \, dE$ is the integrated intensity of an ISS peak. This quantity should scale with the relative proportion of fluorine adatoms that are adsorbed on the topmost layer of the substrate. If there is no spatial redistribution of the fluorine adatoms as a consequence of the annealing procedure, the ratio of the "before" and "after" values will be unity. For five different annealing temperatures between 300 and 700 K, annealing the adlayer was found to have a negligible effect on the distribution of adsorbed fluorine atoms. In particular, the ratio was found to be 0.98 ± 0.11. This was even the case after annealing to 700 K, a procedure which resulted in a partial (~ 20%) decomposition of the adlayer (see section 3.2 below).

3.2. Decomposition / desorption kinetics

3.2.1. Temperature programmed decomposition

The thermal decomposition of silicon-fluoride adlayers, produced by exposing a clean Si(100) surface to a molecular beam of F_2, or a mixture of F_2 and F, have been investigated by employing both XPS and quadrupole mass spectrometry. XPS has been utilized to monitor the depletion of the fluorine adatom concentration as a function of time while the Si substrate is heated at a constant rate. Mass spectrometry has been employed to monitor the rate of desorption of the gas phase reaction products. Since a number of gas phase reaction products can be expected as a consequence of the decomposition reaction [14], by coupling mass spectrometric detection with XPS, we are permitted an accurate determination of the product yields as a function of adlayer composition.

The qualitative features of the thermal decomposition of silicon-fluoride adlayers can be assessed by the data shown in fig. 6. These data were produced by exposing a clean Si(100) surface at a temperature of 120 K to a molecular beam of fluorine (either $10\%F_2$/Ar or $10\%F_2$/He) for a fixed time, and subsequently heating the surface at a constant rate of 0.5 K s^{-1}. Initial fluorine coverages above ~ 2 ML were obtained by thermally dissociating a fraction of the F_2 to F by heating the nozzle of the beam source as described above in section 3.1.3. As may have been expected, for a given initial fluorine adatom concentration, the kinetics of the thermal decomposition was found to be independent of the nature of the incident reactant beam employed to dose the surface (e.g., F_2/He versus F_2/Ar, F_2 versus F). The depletion of the fluorine coverage with increasing temperature depicted in fig. 6 was determined via XPS by monitoring the F(1s) peak at a single fixed energy, as discussed above in section 2.3. Both the apparent and "corrected" coverages, i.e., employing $\theta_\infty = 5.3$ ML, are displayed in fig. 6. Drift in the XPS signal with either time or substrate temperature was assessed by monitoring simultaneously (i.e., by multiplexing the energy analyzer) both the Si(2p) peak and the background level near the F(1s) peak. The measured drift was always less than 5% of the total signal.

Since the heating rates employed here were essentially linear, the abscissa is representative also of time. In regions where there is primarily one gas phase desorption product, differentiation of these curves will yield the rate of desorption, i.e., $r_{des} \propto -d\theta/dt$. Therefore, there should be a one-to-one correspondence between the maxima of $-d\theta/dt$ and the thermal desorption peaks detected by mass spectrometry. As may be seen in fig. 6, there are 3–4 such maxima, i.e., inflection points. For initial coverages below one monolayer, there is a single feature near 800 K, which is present also for all other initial coverages. At an initial coverage of ~ 2 ML, a weak shoulder is apparent near 700 K. At 6–13 ML a sharp feature near 675 K is evident. Finally, for an
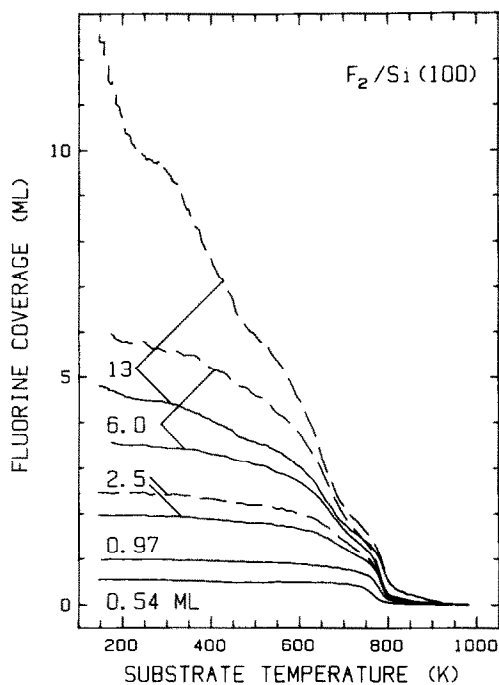
Fig. 6. Temperature-programmed decomposition of silicon-fluoride adlayers produced by expos-
ing a clean Si(100) surface at 120 K to either a beam of F_2 or a mixture of F and F_2. The coverage
was evaluated via XPS, and the initial ("corrected") coverages are designated in each case. The
solid curves represent apparent coverages, whereas the dashed lines represent the "corrected"
coverages calculated by employing the procedure detailed in section 2.3. in all cases, the (constant)
heating rate was 0.5 K s^{-1}.

initial coverage of 13 ML a feature near 450 K is present, in addition to a
measurable rate of decomposition below 200 K.

Thermal desorption spectra of the gas phase reaction products, $SiF_4(g)$
(monitoring SiF_3^+, $m/e = 85$) and $SiF_2(g)$ (monitoring SiF_2^+, $m/e = 66$) de-
tected by the mass spectrometer (electron energy of 110 eV) are shown in fig.
7. Spot checks indicated that neither F_2 ($m/e = 38$) or higher molecular weight
products (e.g., $Si_2F_6(g)$, monitoring $Si_2F_5^+$) were produced under the reaction
conditions considered here. The assignment of the mass spectra shown in fig.
7a and 7b to their corresponding neutral species (i.e., SiF_4 and SiF_2) is based
on the following experimental observations. Mass spectra monitoring SiF^+
($m/e = 47$) were found to be essentially identical to those found for SiF_2^+, the
two sets of spectra differing by a single constant of proportionality in all cases.
On the other hand, no such correlation was found between the SiF_3^+ and SiF_2^+
spectra, suggesting strongly that these fragments were formed from different
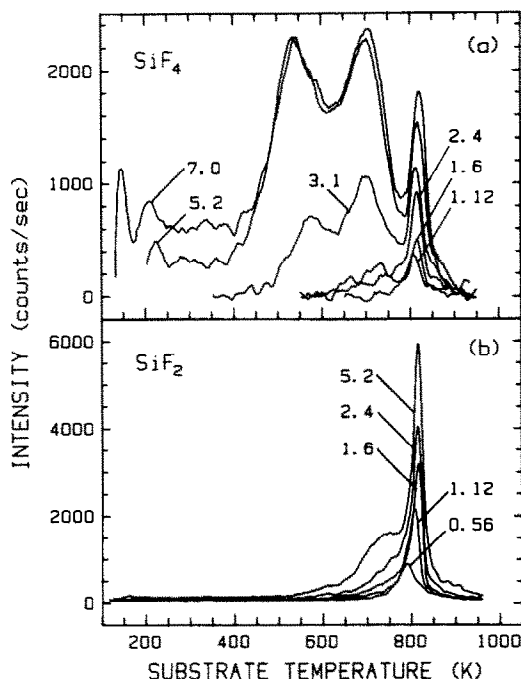parent neutral species. SiF_3^+ is known to be the dominant (~ 90%) cracking

Fig. 7. Temperature-programmed desorption spectra of the gas phase reaction products, (a) SiF_4 and (b) SiF_2, produced from the thermal decomposition of silicon-fluoride adlayers. Fluorine was adsorbed at a substrate temperature of 120 K up to the designated coverages, and the surface was heated at the constant rate of 4 K s^{-1}.

fragment from SiF_4(g) [8,50], whereas SiF_2^+ and SiF^+ are formed in comparable amounts from electron impact ionization of SiF_2(g) [51]. In regards to the latter, the intensity ratio $I_{SiF^+}/I_{SiF_2^+}$ was found here to be equal to 1.2, which, after accounting for the sensitivity of our mass spectrometer, is in fair agreement with the relative ionization cross-sections found for SiF_2(g) [51]. Thus, under the reaction conditions considered here, the only gas phase reaction products produced from the thermal decomposition of silicon-fluoride adlayers were SiF_2(g) and SiF_4(g).

A cursory examination of the thermal desorption spectra given in fig. 7 reveals several features of the decomposition reaction. For both products, there is good agreement between the observed desorption peaks and those predicted by the time-resolved XPS results given in fig. 6. In particular, a single, relatively sharp desorption peak is observed for SiF_2, centered near 800 K. Above initial coverages of ~ 2 ML, a shoulder builds in on the low-temperature side of this peak. For SiF_4 a small sharp peak is centered near 800 K, whereas a broad, two-peaked (~ 550 K and ~ 700 K) feature is dominant for initial coverages above ~ 3 ML. Since gas phase SiF_2 is known to produce
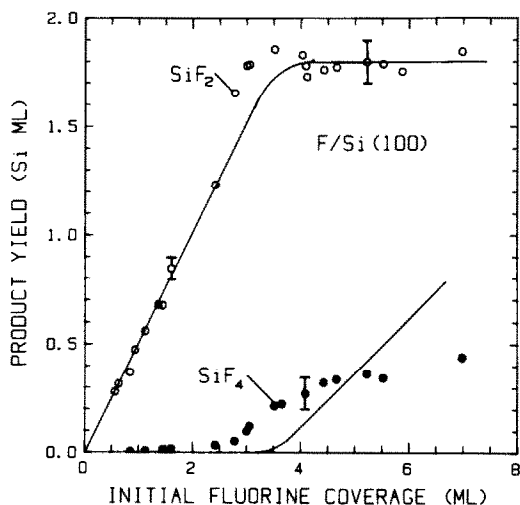
Fig. 8. Desorption product yields from the thermal decomposition of silicon-fluoride adlayers as a function of the initial fluorine adatom coverage, where the fluorine was adsorbed at a substrate temperature of 120 K. The product yields were evaluated by integrating desorption spectra such as those given in fig. 7 and are expressed in terms of monolayers of the *silicon substrate*.

SiF_4 as a result of reactions with stainless-steel chamber walls [8], we cannot totally exclude the possibility that some fraction of the SiF_4 desorption peak near 800 K is actually due to desorbing SiF_2.

In regards to the relative product yields, the mass spectrometric intensities are proportional to the rates of desorption and inversely proportional to the effective pumping speed of the product detected [52]. Consequently, the integrated areas of the peaks are proportional to the relative product yields. Separate measurements indicate that the effective pumping speed for SiF_2 exceeds that for SiF_4 in our experimental arrangement by approximately two orders of magnitude. Thus, assuming comparable mass spectrometric sensitivities for SiF_2 and SiF_4, we conclude that for initial coverages below ~ 2 ML, SiF_2 is the *major* reaction product.

This conclusion is better quantified by the data shown in fig. 8, where we have plotted the product yields, as deduced by integration of thermal desorption spectra, versus the initial fluorine adatom concentration. Note that the product yields are given in terms of monolayers of the *Si substrate*. Since SiF_2 is the major product below initial coverages of ~ 2 ML, determination of the SiF_2 yields was straightforward. The SiF_4 desorption spectra were calibrated by employing a mass balance on fluorine, considering only those cases where the initial coverage was above ~ 3.5 ML. The data given in fig. 8 verify that SiF_2 is the major reaction product below ~ 3 ML, i.e., the functional dependence of the product yields can only be explained if this is the case. In

addition, it is evident that the absolute yield of SiF_2 remains constant above initial coverages of 3 ML, whereas the yield of SiF_4 increases continuously with increasing coverage beyond 3 ML. The data may be compared to a theoretical prediction, given by the solid lines, and based on 100% conversion to SiF_2 for initial coverages ≤ 3.6 ML, and 100% conversion to SiF_4 for the coverage in excess of 3.6 ML. We see there is fair agreement between this prediction and the experimental data. The discrepancies between the model and the data are no doubt due to both the need to correct the coverages as deduced by XPS (at the high concentration), and the presence of a high background intensity for SiF_4 (i.e., SiF_3^+), which made choice of a suitable baseline for integration difficult. Concerning the former, better agreement with the overall mass balance on fluorine could be obtained by employing a value of $\theta_\infty \simeq 4.0$ ML for the coverage correction [53].

Up to this point, we have considered primarily the qualitative aspects of the thermal decomposition of silicon-fluoride adlayers – i.e., which gas phase products are formed, the relative yields as a function of the initial coverage, etc. As may be ascertained from an inspection of figs. 6 and 7, above initial coverages of ~ 2 ML, the kinetics of the thermal decomposition is undoubtedly quite complex. For example, above 2 ML, the two gas phase reaction products are formed simultaneously in certain ranges of temperature, and the multiple peak structure apparent in fig. 7a suggests that there may be several reaction channels leading to the formation of SiF_4. However, below 2 ML, there is essentially only one gas phase reaction product, SiF_2, the formation of which, as implied by the sharp desorption peak centered near 800 K, is apparently a well defined process. Moreover, a crude deconvolution of the SiF_2 desorption feature for coverages above 3 ML, i.e., into a sharp peak at 800 K and a broad peak near 700 K, indicates that the coverage corresponding to the sharp peak is 2 ML, or one monolayer of the silicon substrate. Thus, we may conclude that a more detailed examination of the desorption kinetics of SiF_2 below coverages of 2 ML will lead to insights into the mechanism of the reaction that is responsible for the gasification of a single monolayer of the silicon substrate.

Closer inspection of the thermal desorption spectra of SiF_2 displayed in fig. 7b, especially those representative of initial coverages of fluorine ≤ 2 ML, reveals considerable overlap of the low-temperature, leading edge of these spectra, and the spectra are decidedly asymmetric. This behavior is characteristic of zero-order desorption kinetics [52]. In order to better quantify the kinetics of $SiF_2(g)$ formation, we carried out a series of experiments that involved fixing the initial coverage, and varying the rate at which the surface was heated. This method [54] permits an evaluation of the kinetic parameters at a fixed coverage and, under the appropriate circumstances, a determination of the "order" or molecularity of the surface reaction. In order to evaluate whether the decomposition reaction is "history dependent", the kinetics have
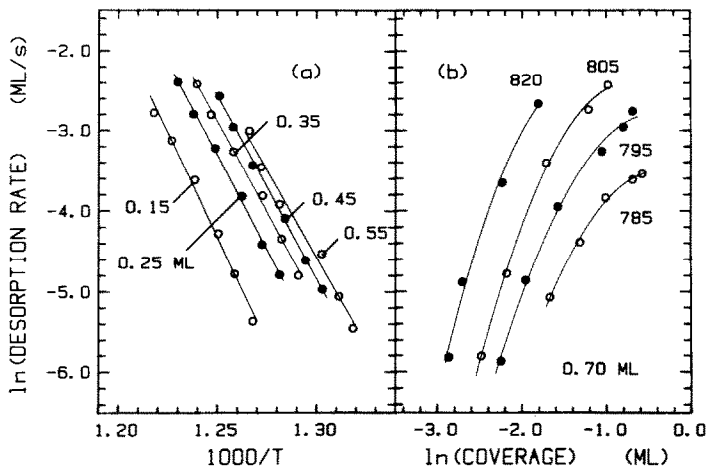
Fig. 9. (a) Arrhenius plots of the rate of SiF₂ desorption versus the reciprocal temperature for five different coverages of fluorine adatoms. (b) "Order plots" of the (ln) rate of SiF₂ versus the (ln) coverage for four different temperatures. In all cases the initial coverage of fluorine adatoms was fixed at 0.70 ML. Note that, in the absence of coverage-dependent kinetic parameters, the slope of the curves in (b) corresponds to the "order" or molecularity of the desorption reaction.

been examined at three different *initial* coverages of fluorine adatoms, namely, 0.70, 1.26 and 2.89 ML. In particular, if a thermodynamic equilibrium is maintained in the adlayer, then the kinetics of the decomposition reaction should be independent of the initial composition and/or configuration of the adlayer. Note that since the decomposition reaction involves removal of Si substrate atoms, a thermodynamic equilibrium involves *both* the adlayer (fluorine adatoms) and the substrate (Si surface atoms). A convenient reference for the three initial coverages considered is the apparent "saturation" coverage at low exposures, i.e., ≈ 1.2–1.6 ML (cf. fig. 2). Thus the three initial coverages investigated represent ~ $\frac{1}{2}$, 1 and 2 times this "saturation" value.

Arrhenius plots of the rate of desorption versus the reciprocal temperature, constructed from desorption spectra of SiF₂ similar to those shown in fig. 7b, and produced by employing seven different heating rates varying between 0.5 and 10 K s^{-1}, are shown in figs. 9a, 10a and 11a, which correspond to initial coverages of fluorine of 0.70, 1.26 and 2.89 ML, respectively. Note that in the latter case 2.08 ML of the adsorbed fluorine adatoms were converted to SiF₂(g). We see that in all cases the rates of desorption are described well by an Arrhenius expression. "Order plots" of the (ln) rate of desorption versus the (ln) fluorine coverage at a fixed temperature are shown in figs. 9b, 10b and 11b, these data derived from the identical spectra utilized in the Arrhenius constructions. In the absence of coverage-dependent kinetic parameters (i.e.,
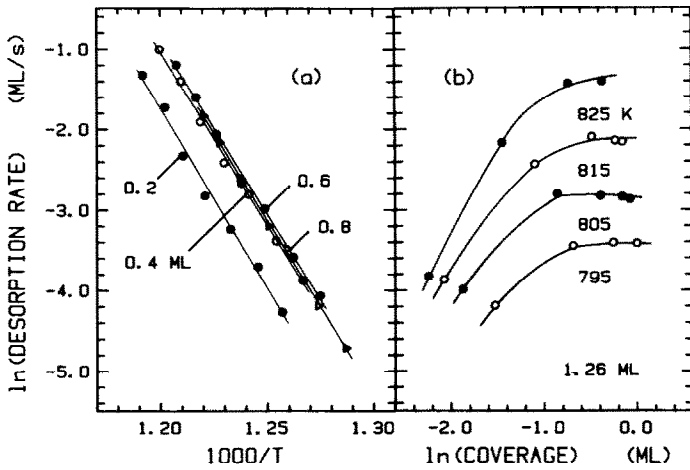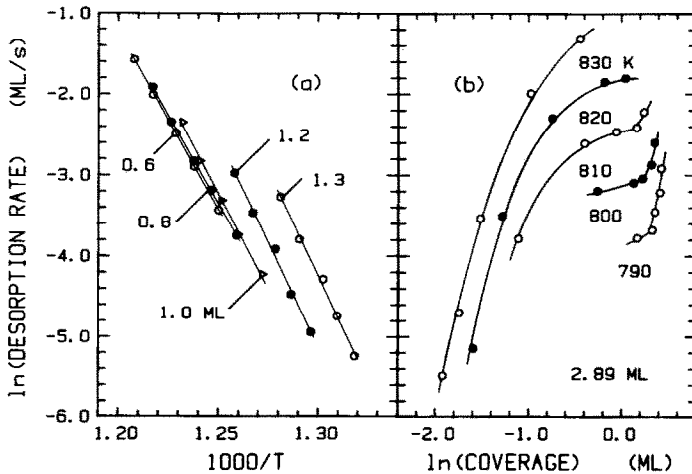
Fig. 10. (a) Arrhenius plots of the rate of SiF$_2$ desorption versus the reciprocal temperature for four different coverages of fluorine adatoms. (b) "Order plots" of the (ln) rate of SiF$_2$ versus the (ln) coverage for four different temperatures. In all cases the initial coverage of fluorine adatoms was fixed at 1.26 ML.

the activation energy and the preexponential factor) the slope of these curves will reflect directly the "order" of the reaction, i.e. $\partial \ln r_{des}/\partial \ln \theta_F$ [55].

Examination of figs. 9b, 10b and 11b indicates that the "order" of the decomposition reaction is dependent upon the initial coverage of fluorine

Fig. 11. (a) Arrhenius plots of the rate of SiF$_2$ desorption versus the reciprocal temperature for different coverages of fluorine adatoms. (b) "Order plots" of the (ln) rate of SiF$_2$ versus the (ln) coverage for four different temperatures. In all cases the initial coverage of fluorine adatoms was fixed at 2.89 ML.

adatoms. For example, for an initial coverage of 0.70 ML the reaction is positive order for all coverages considered, with the apparent order decreasing with increasing coverage. Since the kinetic parameters are dependent on coverage in this range it is difficult to assign a specific value for the order of reaction, although, in the limit of low coverages, it appears to be nearly second-order. The situation is quite different for an initial coverage of 1.26 ML. Below ~ 0.3 ML the reaction is again positive order, however, zero-order kinetics are indicated between coverages of ~ 0.4 and 1.0 ML. For an initial coverage of 2.89 ML, the kinetics are even more complicated. In particular three regimes are evident – positive order below ~ 0.6 ML, zero-order between 0.6 and 1.0 ML, and large positive order above 1.0 ML. These results are somewhat surprising for a reaction as "simple" as thermal decomposition of a silicon-fluoride adlayer, which produces essentially a single reaction product, $SiF_2(g)$, at low coverages.

The Arrhenius constructions shown in figs. 9a, 10a and 11a can of course be utilized to derive the kinetic parameters that describe the reaction leading to the desorption of SiF_2. Since zero-order kinetics has been implicated for a wide range of coverages, especially for an initial coverage of 1.26 ML, for convenience we shall assume that the rate of desorption is given by

$$r_{des} = k_{d,0}^{(0)} \exp(-E_d/k_B T),$$

where $k_{d,0}^{(0)}$ is the (apparent) zero-order preexponential factor in ML s^{-1}, and E_d is the activation energy. This assumption does not affect the evaluation of the activation energy, whereas the apparent zero-order preexponential factor can be related to a generalized nth order preexponential factor via $k_{d,0}^{(0)} \equiv \theta^n k_{d,n}^{(0)}$. The values derived from the data are plotted in fig. 12 as a function of fluorine adatom coverage. As may be seen, the kinetic parameters are nearly independent of coverage (both "instantaneous" and initial) between ~ 0.4 and 1.0 ML, and the mean values for an initial coverage of 1.26 ML are given by $k_{d,0}^{(0)} = 1.4 \times 10^{22 \pm 1}$ ML s^{-1} and $E_d = 86 \pm 2$ kcal mol^{-1}. For an initial coverage of 0.70 ML, however, the kinetic parameters display a definite dependence on coverage, increasing significantly as the coverage decreases. The kinetic parameters representative of an initial coverage of 2.89 ML also display a dependence on coverage, increasing with increasing coverage above ~ 0.90 ML. In both cases where a dependence on coverage is evident, the kinetic parameters compensate significantly for one another, i.e., the often observed, but poorly understood "compensation effect".

Since the formation of $SiF_4(g)$ is of considerable importance to the "low" temperature (i.e., 300–400 K) etching of silicon by fluorine molecules and/or atoms [6,23,25] we have attempted a quantitative analysis of the SiF_4 thermal desorption spectra. Unfortunately, our analysis was hampered by the low pumping speed for $SiF_4(g)$ [i.e., compared to $SiF_2(g)$], which precluded a rigorous analysis [54] of the data such as those portrayed in figs. 9b, 10b and
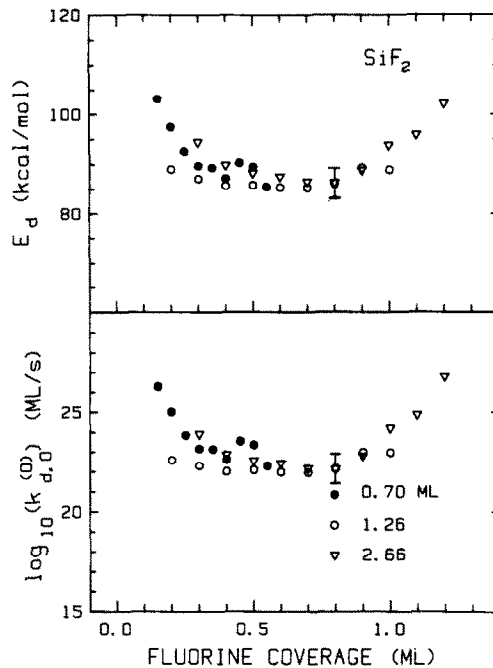
Fig. 12. Activation energy (E_d) and apparent zero-order preexponential factor ($k_{d,0}^{(0)}$) describing the rate of SiF$_2$ desorption as a function of fluorine adatom coverage for three different *initial* coverages of fluorine.

11b for SiF$_2$(g). In particular, the low pumping speed for SiF$_4$(g) limited the range of useful heating rates, and was manifest also in a lower signal-to-noise ratio due to a high background pressure of SiF$_4$(g). Two approaches to a quantitative analysis were attempted – the first involved fitting the entire desorption peak to an analytical expression valid for either first- or second-order kinetics, whereas the second involved an analysis of the variation in the peak temperature with the linear heating rate [52]. Both analyses are rigorous provided: (a) the kinetic parameters are independent of coverage; (b) a constant order of reaction is observed; and (c) the desorption peak is representative of a single reaction channel, i.e., it is not a superposition of several, competing reaction channels. Since the desorption spectra for SiF$_4$ are dominated by the two-peaked structure appearing between 400 and 800 K, this feature was analyzed as arising from two parallel reaction channels. The desorption peak appearing near 800 K was not analyzed since, as discussed above, it may be associated with the desorption of SiF$_2$(g).

The analysis based on fitting the entire desorption peak is dependent upon assigning a particular order to the desorption reaction. Both the full-width at half maximum (FWHM) of the desorption peak and the variation of the peak

temperature with increasing coverage can be used to deduce the reaction order. In particular, the FWHM's of the two peaks considered here are ~ 100 K, which, for these peak temperatures, suggest second-order kinetics. In addition, as the initial coverage increases from 3.3 to 5.9 ML, the peak temperatures shift to lower values, i.e., from ~ 725 and 588 K to 703 and 553 K, which is also indicative of second-order kinetics. Consequently, in the nonlinear least-squares fitting procedure, both reaction channels were assumed to be second-order. From the analysis of three separate spectra, similar to those given in fig. 7b and representative of an initial coverage of 3.3 ML, the (mean) optimal parameters were found to be $E_d = 32 \pm 3$ kcal mol^{-1} and $k_{d,1}^{(0)} = 5 \times 10^{8 \pm 1}$ s^{-1} for the desorption peak near 700 K, and $E_d = 17 \pm 3$ kcal mol^{-1} and $k_{d,1}^{(0)} = 2 \times 10^{5 \pm 1}$ s^{-1} for the peak near 550 K. An analysis of spectra representative of initial coverages of 5.9 ML and above gave similar (i.e., within experimental error) kinetic parameters. Note that, in these cases, $k_{d,1}^{(0)}$ is the equivalent first-order preexponential factor, viz., $k_{d,1}^{(0)} \equiv \theta_0 k_{d,2}^{(0)}$, where θ_0 is the initial coverage and $k_{d,2}^{(0)}$ is the second-order preexponential factor. In practice, it was found that assuming the peak at 550 K exhibited second-order kinetics, whereas the peak at 700 K was first-order gave an equally good fit to the data. In these cases the optimal parameters were found to be $E_d = 23 \pm 3$ kcal mol^{-1} and $k_{d,1}^{(0)} = 7 \times 10^{5 \pm 1}$ s^{-1}, and $E_d = 18 \pm 3$ kcal mol$^-$ and $k_{d,1}^{(0)} = 8 \times 10^5 \pm 1$ s^{-1} for the two desorption peaks respectively.

The analysis examining the variation in the peak temperature with the linear heating rate involves plotting the quantity $\ln(\beta/T_p^2)$ versus $1/T_p$, where β is the linear heating rate and T_p is the peak temperature [52]. One obtains the quantity $-E_d/k_B$ from the slope and the quantity $k_{d,1}^{(0)}/(E_d/k_B)$ from the intercept. An analysis of four separate spectra produced by heating rates of 4.0, 2.8, 1.5 and 0.8 K s^{-1} and representing an initial coverage of 3.3 ML gave kinetic parameters of $E_d = 45 \pm 9$ kcal mol^{-1} and $k_{d,1}^{(0)} = 6 \times 10^{12 \pm 4}$ s^{-1} for the desorption peak near 700 K, and $E_d = 23 \pm 6$ kcal mol^{-1} and $k_{d,1}^{(0)} = 4 \times 10^{7 \pm 2.5}$ s^{-1} for the peak near 550 K. These values are only in fair agreement with those determined from fitting the entire desorption peak, although they are within the experimental uncertainties, which are quite large in these cases.

3.2.2. Isothermal decomposition

As an independent check of the analysis described above in section 3.2.1 utilizing thermal desorption spectra of SiF$_2$, we have investigated also the isothermal decomposition of silicon-fluoride adlayers by employing XPS to monitor the time-dependent fluorine adatom concentration. These experiments involved exposing the clean Si(100) surface to a flux of fluorine at a temperature well below 800 K, extinguishing the beam, and subsequently heating the surface rapidly to the desired temperature, which was typically near 750–800 K. The fluorine coverage was determined by monitoring the
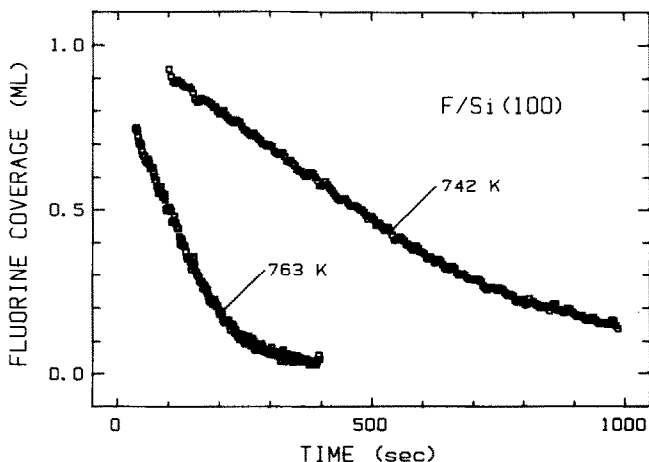
Fig. 13. Isothermal decomposition of a silicon-fluoride adlayer. The coverage of fluorine was determined via XPS. In both cases, the surface held at a temperature near 600 K was exposed to F_2 until a coverage of ~1 ML was obtained, the beam was extinguished, and the surface was heated rapidly (~10 s) to the indicated temperature. Note the essentially linear decrease in the coverage between 1.0 and 0.3 ML.

F(1s) peak via XPS. Two representative experiments are shown in fig. 13, where the initial coverage was ~1 ML. First of all, an initial acceleratory region is not observed for this initial coverage. Most importantly, it can be seen clearly that between coverages of ~0.3 and 0.9 ML the decrease in the coverage with time is essentially linear, i.e., exactly what is expected from zero-order kinetics. In addition, the decrease in the rate of decomposition for coverages below 0.3 is consistent with a transition to positive -order kinetics in the limit of low coverages, as observed above in fig. 10b.

The experimental data corresponding to the zero-order kinetics regime have been fit by a least-squares routine in order to evaluate the zero-order rate coefficient. An Arrhenius plot of the rate coefficients determined from four separate experiments, including those depicted in fig. 13, was found to be very linear (see fig. 26 below). The corresponding kinetic parameters determined from this construction are given by $k_{d,0}^{(0)} = 1.4 \times 10^{17 \pm 1}$ ML s^{-1} and $E_d = 68 \pm 5$ kcal mol^{-1}. These values are only in fair agreement with those determined from mass spectrometry, i.e. those given in fig. 12. However, the range of surface temperatures examined by the two techniques differed – the thermal desorption results were confined to approximately $T_s = 780$–835 K, whereas the XPS results are representative of $T_s = 740$–805 K. Moreover, in the range of temperatures common to both analyses, the rate coefficients determined from the two techniques were within a factor of 1.5 of each other. Possible explanations for this apparent discrepancy between the two sets of kinetic parameters measured here are discussed below (see section 4.2).

3.2.3. Modulated F_2 beam experiments

Several experiments have been conducted employing a modulated flux of F_2 incident on the Si(100) surface while monitoring simultaneously either the fluorine adatom concentration via XPS, or the desorbing flux of the gas phase reaction products via quadrupole mass spectrometry. In regards to the latter, commonly referred to as modulated molecular beam reactive scattering (MMBRS), a Fourier analysis of the waveform(s) of the desorbing gas phase product(s) flux detected by the mass spectrometer can yield kinetic information (e.g., rate coefficients) directly [56, 31]. Unfortunately, such an analysis encounters nontrivial difficulties in the examination of nonlinear reaction kinetics [e.g., a second-order reaction, which is suggested here for $SiF_2(g)$ formation at low coverages by the data shown in figs. 9–11 [57]. Nevertheless, in certain "simple" nonlinear cases [58], by assuming a particular kinetic model a Fourier analysis is capable of extracting reaction rate coefficients.

The formation and decomposition of silicon-fluoride adlayers, representative of the monolayer regime, have been examined by modulating the incident F_2 beam flux and monitoring the fluorine coverage via XPS. Three representative experiments, distinguished by differing substrate temperatures and modulation periods, are displayed in fig. 14 where the fluorine coverage is plotted as a function of dimensionless time, i.e., the time divided by the modulation time period. The F_2 beam flux is the same in all cases, and each curve is the summed average of four consecutive waveforms. For a temperature of 789 K, there is rapid increase in the coverage following exposure to the beam followed
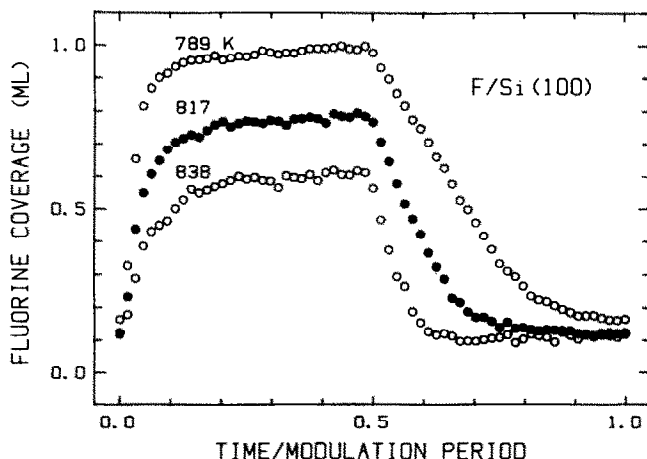

Fig. 14. XPS waveforms for three different substrate temperatures produced by square-wave modulating the incident F_2 flux and measuring simultaneously the fluorine adatom coverage by monitoring the F(1s) peak. To facilitate the presentation, the abscissa represents the fractional modulation time period, where the time period in each case was 134 s (789 K), 55 s (817 K) and 39 s (838 K).

by a gradual approach to the "steady-state" coverage, and finally a relative slower decay in the coverage subsequent to the extinguishing of the beam. Consistent with the data given in fig. 13 above, there is a linear decrease in the coverage after the beam is turned off, the linear portion extending between ~ 1.0 and 0.3 ML. An analysis of these data in the zero-order regime gives rate coefficients that are in excellent agreement with those determined above from isothermal decomposition (see section 3.2.2). It is also apparent that the "steady-state" coverage reached in each case decreases with increasing substrate temperature. This observation is explained readily by solving the surface mass balance for the coverage of fluorine adatoms. If we assume that the rate of adsorption is given by that found at a substrate temperature of 600 K, i.e., $r_{ads} = S_0 F_{F_2}(1 - \theta_F/\theta_{F,sat})^2$, and the rate of desorption of SiF_2 is given by that found for the zero-order regime (valid for $\theta_F \geq 0.3$ ML and initial coverages of $\simeq 1$ ML), i.e., $r_{des} = k_{d,0}(T) \equiv k_{d,0}^{(0)} \exp(-E_d/k_B T)$, the steady-state coverage $\theta_{F,s}$ is given by

$$\theta_{F,s} = \theta_{F,sat}\left[1 - \left(k_{d,0}/S_0 F_{F_2}\right)^{1/2}\right].$$

Thus, since the rate coefficient k_d increases with increasing temperature, at a constant flux the steady-state coverage will decrease with increasing temperature. Employing the zero-order rate coefficients determined in section 3.2.2, we find that the variation of the steady-state coverages with temperature observed in fig. 14 is in good agreement with this expression.

The kinetics of the formation of SiF_2 is the limit of very low coverages, i.e., below ~ 0.01 ML, has been examined via MMBRS. As stated above, this technique is quite useful in the examination of linear surface reaction kinetics. Moreover, provided the nature of the nonlinearity is relatively simple and can be deduced a priori, analysis of nonlinear systems via MMBRS can also be employed successfully. Since we shall examine here only the limit of very low coverages, the coverage-dependence of both the adsorption kinetics (i.e., $r_{ads} \simeq S_0 F_{F_2}$ for $\theta/\theta_{sat} \ll 1$) and the kinetic parameters can be safely neglected. If this were not the case, the resulting complexity of the nonlinearities would undoubtedly rule out any quantitative analysis via MMBRS. Thus, the only expected nonlinearity is that due to the surface reaction leading to the desorption of SiF_2, which, as suggested by the thermal decomposition results [cf. fig. 10b], is probably second-order.

Three waveforms of the desorbing SiF_2 flux, detected by the mass spectrometer and representative of different substrate temperatures, are shown in fig. 15. The F_2 beam flux was the same in all cases and each curve is the summed average of waveforms acquired over a 1000 s time period. If we assume both the angular and velocity distributions of the desorbing flux are only weak functions of the substrate temperature (i.e., for this temperature range), these mass spectrometric intensities acquired at a fixed angle are
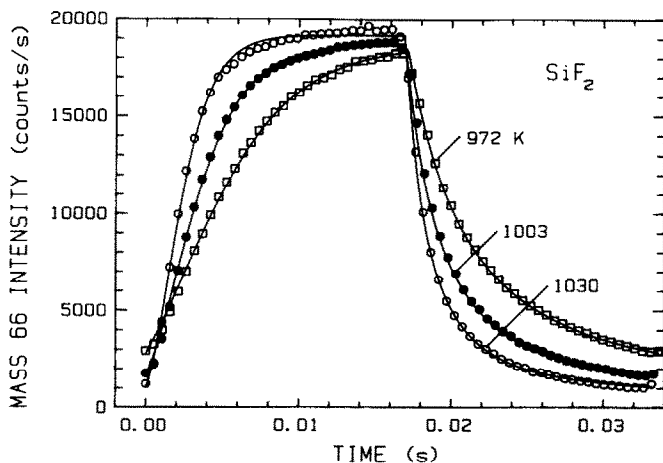
Fig. 15. QMS waveforms for three different substrate temperatures produced by square-wave modulating the incident F_2 flux and measuring simultaneously the desorbing SiF_2 flux. The estimated mean coverage of fluorine adatoms under these conditions was much less than 0.01 ML. The solid curves represent least-squares fits to the integrated form of the surface mass balance equation [see text and eq. (3)], where the assumption of second-order kinetics provided a superior fit to the data. The experimental uncertainties are indicated by the size of the plotted symbols.

simply proportional to the rate of desorption. The effect of substrate temperature on the surface reaction is clearly evident, e.g., for the lower substrate temperatures the waveforms are increasingly damped or "demodulated", consistent with a rate of reaction increases with increasing temperature. On the other hand, the steady-state reaction probability, which is simply proportional to the peak-to-peak amplitude at sufficiently low frequencies, is very nearly the same in all three cases. We have chosen to analyze these waveforms in two different fashions – the first method involves fitting these curves to the appropriate integrated forms of the surface mass balance on fluorine, whereas the second involves a Fourier analysis.

The waveforms displayed in fig. 15, in addition to others not presented here, have been fit to an integrated form of the mass balance on adsorbed fluorine atoms given by

$$d\theta_F/dt = S_0 F_{F_2}(t) - k_{d,n}\theta_F(t)^n, \tag{3}$$

where $k_{d,n}$ is the nth-order desorption rate coefficient, and $n = 1$ or 2. We shall assume that the incident flux waveform $F(t)$ is given by a square wave, i.e., $F(t) = F_0$ for $0 \leq t \leq T/2$, and $F(t) = 0$ for $T/2 \leq t \leq T$, where T is the modulation time period. The legitimacy of this assumption, e.g., the possible effects of the "chopper gating function", is considered below. The predicted waveforms, which the data were fit to, were obtained by integrating eq. (3)

successively, beginning with the initial condition $\theta_F|_{t=0} = 0$, until satisfactory convergence was achieved, i.e., such that $\theta_F|_{t=0} = \theta_F|_{t=T}$. In all cases a superior fit to the data was provided by assuming that the surface reaction is second-order in θ_F, i.e., $n = 2$. The results of these fits, produced by a nonlinear least-squares procedure, are displayed in fig. 15, where the quantity plotted is proportional to the desorbing product flux, i.e., $k_{d,n}\theta_F(t)^n$. We see that the agreement between this model and the experimental data is excellent.

The validity of this fitting procedure can be checked by comparing the Fourier coefficients of the predicted and measured waveforms. For example, one might intuitively expect that the least-squares fitting procedure employed above is weighted towards the "low" frequency components of the waveforms displayed in fig. 15. In particular, it can be shown that the high frequency components are most sensitive to those portions of the waveform where the rate of reaction is changing rapidly. Thus, a more complete examination of the waveforms in the frequency domain would provide a more rigorous test of the proposed model. The amplitude and phase of the first 16 coefficients of the predicted and measured waveforms are displayed in fig. 16 as a function of the radial frequency. The most obvious feature to note from this figure is the relative magnitude of the even order coefficients. In particular, since a square wave does not contain even order components, the appearance of even order components in the product waveform (which are obviously well above the noise level) verifies the presence of nonlinear surface reaction kinetics. In regards to the particular nonlinearity assumed here, i.e., a second-order reaction, the agreement between the predicted and measured coefficients is excellent up to approximately the tenth harmonic. The deviation between the model and the data beyond there is probably primarily due to the effect of the chopper gating function. This is reasonable since we estimate the width of the gating function to be ≤ 2 ms, i.e. $\leq T/10$.

The data given in fig. 16 may also be used to evaluate the kinetic parameters. Since the reaction kinetics is nonlinear, the values obtained from a Fourier analysis will represent *apparent* kinetic parameters. However, provided certain conditions are met, these values can be utilized to obtain the true values. To proceed with a Fourier analysis one employs eq. (3) and assumes that

$$F_{F_2}(t) = \tfrac{1}{2}F_0\left(1 + \xi_1 \, e^{i\omega t} + \xi_3 \, e^{i3\omega t} + \cdots \right)$$

and

$$\theta_F = \vartheta_0 + \vartheta_1 \, \exp^{i\omega t} + \vartheta_2 \, \exp^{i2\omega t} + \cdots,$$

where for square-wave modulation $\xi_n = 2/n\pi$. From the zero-order equation (i.e., $\omega = 0$) one finds that the mean coverage is given by $\vartheta_0 = (S_0 F_0/2k_d^{(2)})^{1/2}$. Similarly, from the first-order equation one finds that the rate of desorption at
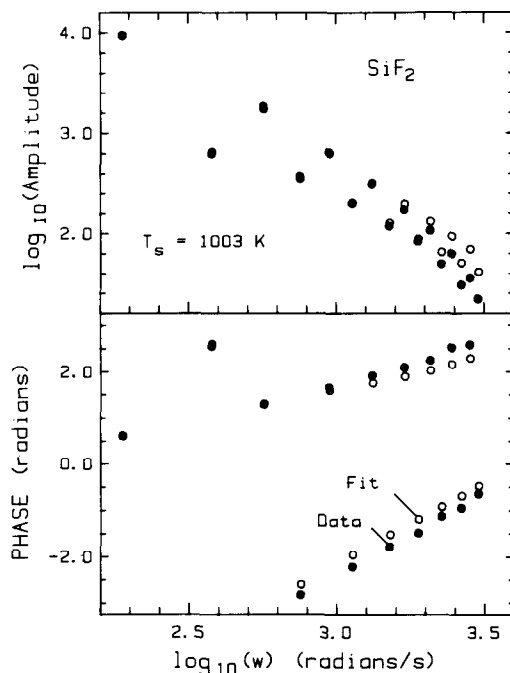
Fig. 16. Bode plot of the first 16 Fourier coefficient of the QMS waveform obtained at a substrate temperature of 1003 K and displayed above in fig. 15. The filled circles represent the Fourier coefficients derived from the experimental data, whereas the open circles represent those obtained from the analytic fit displayed in fig. 15. Note that for pure square-wave modulation and linear surface reaction kinetics, the even order coefficients will identically be equal to zero (practically, equivalent to the noise level). Thus, significant amplitudes for even order coefficients signal a nonlinear reaction mechanism.

the fundamental frequency is given by

$$k_{d,2}\theta_F(\omega)^2 = k_{d,2}(2\vartheta_0\vartheta_1) = \frac{\xi_1(S_0F_0/2)}{1 + i(\omega/k_{app})}, \tag{4}$$

where the *apparent* rate coefficient $k_{app} = 2k_{d,2}\vartheta_0$. Note that the apparent rate coefficient is a function of both the reaction probability S_0 and the incident flux F_0. Consequently, one cannot speak of a "system transfer function" that will relate the incident and product waveforms in all cases, independent of S_0F_0. One can continue in this manner and conceivably calculate all of the coefficients ϑ_n, however, there is little point in doing so since the apparent rate coefficient may be found from an analysis of solely the response at the fundamental frequency [i.e., eq. (4)] [59]. In particular, the phase is given by $\phi(\omega) = -\tan^{-1}(\omega/k_{app})$.
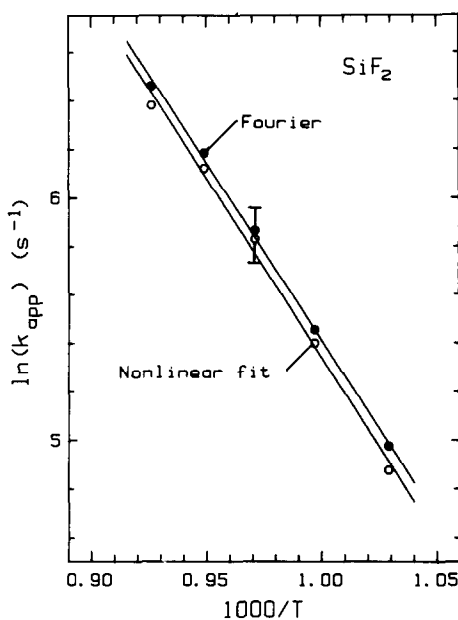
Fig. 17. Arrhenius plots of the apparent reaction rate coefficients derived from the analytic fits displayed in fig. 15 (filled circles), and from an analysis employing only the first Fourier coefficient [open circles, see text and eqs. (4) and (5)]. For second-order kinetics the slope of these curves is equal to $-E_d/2k_B$.

As stated above, the apparent rate coefficient is a function of S_0F_0. An examination of the waveforms displayed in fig. 15 suggests that this quantity is nearly constant for these experiments. This is supported by the fitting procedure employed above – specifically, S_0F_0, which was a fitting parameter, was found to vary by less than 10%. Consequently, an Arrhenius plot of the apparent rate coefficients versus reciprocal temperature, at a fixed flux and a constant reaction probability, will yield kinetic information, viz.

$$k_{app} = \left(2k_{d,2}S_0F_0\right)^{1/2} \equiv \left(2S_0F_0k_{d,2}^{(0)}\right)^{1/2} \exp\left(-E_d/2k_BT\right), \tag{5}$$

where $k_{d,2}^{(0)}$ is the second-order preexponential factor and E_d is the activation energy. Thus, the activation energy can be evaluated directly and, provided either S_0F_0 or the mean coverage ϑ_0 is known, the preexponential factor may be evaluated also. Apparent rate coefficients obtained via both the nonlinear fitting procedure and the Fourier analysis are displayed in fig. 17. The linear Arrhenius behavior is evident. In addition, the agreement between the values obtained for the apparent rate coefficients via the two methods is excellent. From the data of fig. 17 we obtain an activation energy of 59 ± 5 kcal mol^{-1}. Estimating our incident flux for these experiments as 0.5 ML s^{-1}, an ap-

proximation good to a factor of three, and employing $S_0 = 0.46$ (see section 3.1.2) we obtain a preexponential factor of 1.2×10^{18} ML^{-1} s^{-1}, or employing a density of $n_s = 6.8 \times 10^{14}$ adatoms cm^{-2} ML^{-1}, 1.7×10^3 cm^2 s^{-1}.

3.2.4. Spatial extent of thermal decomposition

We have attempted a qualitative examination of the spatial extent of the thermal decomposition of silicon-fluoride adlayers representative of the monolayer regime. Such an examination is especially important with respect to the observation here of zero-order kinetics, which were found to span a large coverage range, i.e., between ~ 1.0 and 0.3 ML for initial coverage of $\simeq 1$–1.3 ML. For example, previous work, which examined the desorption of Xe from a W(110) surface [60], has suggested that the observation of zero-order kinetics in the monolayer regime could be explained by the presence of two-dimensional adatom "islands". Several models involving adatom islands that could result in zero-order kinetics were postulated. Since island formation is inherently inhomogeneous, an investigation of the spatial extent (i.e., homogeneous versus inhomogeneous) of the thermal decomposition is most desirable in order to obtain a better understanding of the decomposition reaction.

Fortunately, in the absence here of a direct structural probe, the configuration of the adlayer may be assessed qualitatively by examining the *adsorption* kinetics of F_2 on a partially decomposed adlayer. This is possible since the kinetics of F_2 adsorption on the clean Si(100) surface have been found here to be described by a second-order Langmuir model for substrate temperatures of 300 K and above (see section 3.1.1). Thus, the probability of dissociative adsorption is controlled by the availability of two nearest-neighbor (nn) vacant adsites. The relative population of nn vacant adsites will differ for the limiting cases of a homogeneous, uniformly, randomly distributed adlayer, and an inhomogeneously adlayer composed of separate domains where the *local* coverage of fluorine is either zero or near saturation. In particular, for a coverage of $\theta_F/\theta_{F,sat} = 1 - f$, where f is the fraction of all vacant sites, the probability of adsorption in the homogeneous case will be proportional to f^2, whereas in the inhomogeneous case it will be proportional to f.

The coverage of fluorine, evaluated by XPS, is displayed as a function of exposure in fig. 18a for F_2 adsorbed on a partially decomposed silicon-fluoride adlayer. This surface was produced by adsorbing ~ 1.3 ML of fluorine on a clean Si(100) surface at 300 K, heating to a temperature near 800 K for ~ 20 s, and cooling rapidly to 300 K prior to additional exposure. Essentially identical results were obtained for a surface held at 600 K for both exposures. This experiment presupposes that upon cooling the surface to 300 K (or 600 K), the adlayer configuration present at the higher temperature is "locked in", a supposition that is reasonable provided the rate diffusion of fluorine is negligible during the cooling of the substrate to 300 K. The two curves represent theoretical predictions based on utilizing parameters representative
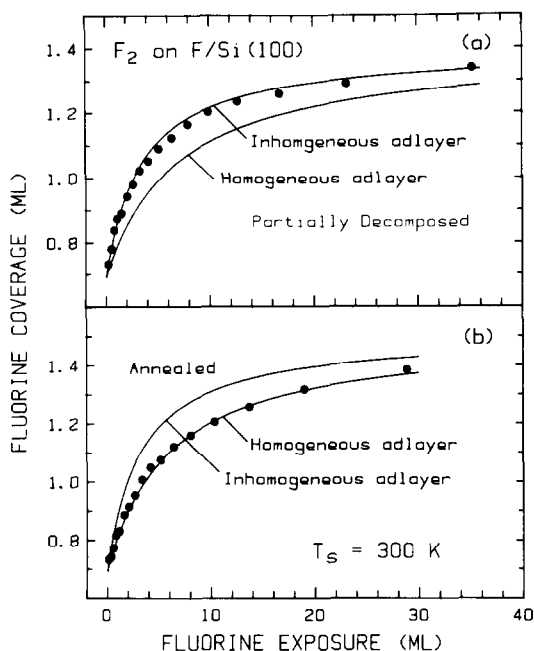
Fig. 18. (a) The coverage–exposure relationship for the adsorption of F_2 on a *partially decomposed* silicon-fluoride adlayer. (b) The coverage–exposure relationship for the adsorption of F_2 on a silicon-fluoride adlayer that was *annealed* to 700 K. The coverages were determined via XPS. The solid lines represent theoretical predictions based on the kinetic parameters found for the clean surface and employing two different models for the adlayer configuration following partial decomposition (see text). The experimental uncertainties are indicated by the size of the plotted symbols.

of the clean surface and assuming that the decomposition proceeds (a) homogeneously, and (b) inhomogeneously, Clearly, the data are represented best by the latter model, suggesting strongly that the thermal decomposition of a silicon-fluoride adlayer proceeds inhomogeneously, leaving separate domains of clean surface and a (locally) saturated adlayer.

It is of interest to determine the nature of the driving force for this apparent domain formation. For example, is domain formation an intrinsic manifestation of the decomposition reaction itself, or is it merely a conse-quence of a thermodynamically favored adlayer configuration? If the latter explanation is important, then simply annealing an adlayer representative of the submonolayer regime to a temperature near the onset of decomposition might lead to domain formation. A representative experiment is shown in fig. 18b, where ~ 0.7 ML of fluorine was adsorbed at a substrate temperature of 300 K, the surface was heated to ~ 700 K, cooled rapidly to 300 K, and exposed subsequently to a constant flux of F_2. The theoretical predictions

based on the two models for the adlayer configuration are shown also in fig. 18b. In this case, the data are described better by the homogeneous model. Thus, these data suggest that the driving force for domain formation is not thermodynamic, rather, it is an intrinsic manifestation of the decomposition reaction itself.

3.2.5. Steady-state thermal decomposition

The steady-state reaction between gas phase F_2 and the Si(100) surface, which leads to the gasification of the Si substrate, i.e., etching, has been examined as a function of substrate temperature. The relative rates of production of the gas phase species have been monitored via mass spectrometry, and the corresponding steady-state coverage of fluorine adatoms has been monitored via XPS. Simultaneous knowledge of the fluorine coverage and the rate of desorption of the products will be decisive in verifying that the F_2 molecules must adsorb dissociatively in order for the etching reaction to occur. That is, these measurements should be able to discount any major rate of reaction occurring via an Eley–Rideal mechanism, i.e., a "direct" reaction between *gas phase* F_2 and the Si(100) surface. For example, for a Langmuir–Hinshelwood mechanism involving reactions of adsorbed fluorine adatoms, the rates of dissociative adsorption of F_2 and desorption of the gas phase products must be equal at steady-state. Since we can predict the rate of dissociative adsorption as functions of both coverage and substrate temperature (see section 3.1.1), the predicted equality of rates can be explicitly verified.

The steady-state values of both the rate of desorption of SiF_2 and the coverage of fluorine adatoms are shown in fig. 19 as functions of the substrate temperature. Under these reaction conditions, the only gas phase reaction products detected were SiF_2 and SiF_4, with SiF_2 being the dominant gas phase reaction product. Based on a correction of the absolute mass spectrometric intensities for the relative pumping speeds (see section 3.2.1), we were able to conclude that the rate of SiF_2 production exceeded that for SiF_4 by at least a factor of 200 for all reaction conditions shown in fig. 19. The close connection between the steady-state coverage and the rate of desorption is clearly apparent. In particular, below ~ 800 K, the coverage is near saturation (~ 1.6 ML) and the rate of SiF_2 desorption is nearly zero. As the substrate temperature is increased slightly above 800 K there is a precipitous drop in the fluorine coverage and, concomitantly, a rapid increase in the rate of reaction. Above a temperature of 900 K the coverage remains nearly zero, whereas the rate of reaction decreases somewhat. As referred to above, the measured rate of reaction can be compared qualitatively to the predicted value by utilizing the measured coverages of fluorine and employing the rate expressions deduced above that describe the adsorption kinetics of F_2 [e.g., eq. (1), where $d = 2$]. In particular, the predicted value is given by $S_0 F_{F_2} (1 - \theta_F/\theta_{sat})^2$, where we set $S_0 F_{F_2}$ equal to the (maximum) SiF_2 intensity observed here at
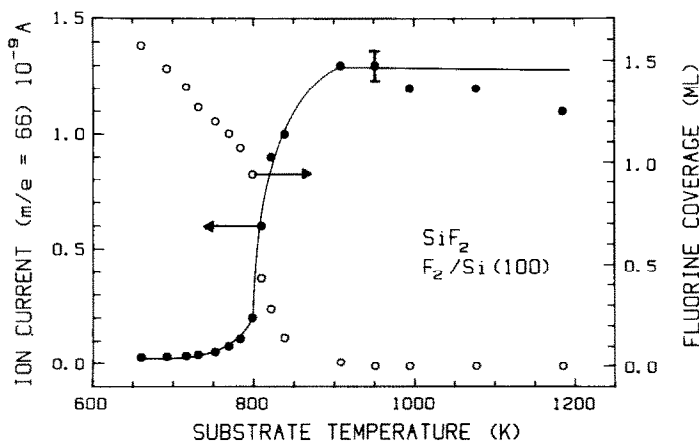
Fig. 19. Steady-state reaction of F_2 with the Si(100) surface as a function of the substrate temperature. The filled circles are proportional to the steady state rate of SiF_2 desorption, the major gas phase reaction product under these conditions. The open circles represent the steady-state coverage of fluorine adatoms as determined via XPS. The solid line represents the theoretical prediction of the SiF_2 desorption rate based on the equality to the rate of dissociative adsorption of F_2 at steady-state, the measured adsorption kinetics [fig. 2 and eq. (1)] and the measured steady-state coverages.

900–950 K. The predicted values are represented by the solid curve displayed in fig. 19. The agreement between the predicted and measured values is excellent. Thus, under the reaction conditions considered here, the dominant reaction pathway leading to the production of $SiF_2(g)$ involves a reaction between adsorbed fluorine adatoms and the Si surface atoms.

3.2.6. Ion-enhancement of $F_2 / Si(100)$ reaction

The effects of a high-energy ion beam on the reaction of F_2 with the Si(100) surfaces has been investigated by exposing the Si(100) surface to both a modulated molecular beam of F_2 and a coincident (constant flux) beam of 1.5 keV Ar^+ ions, while monitoring simultaneously the fluorine coverage via XPS. Due to geometrical constraints associated with the relative positions of the quadrupole, the ion gun, and the Si sample, we were unable to detect gas phase reaction products while the ion beam was incident on the sample. Consequently, a certain amount of ambiguity will be associated with any results obtained from these experiments. In particular, we report here measurements of the accumulation and depletion of the coverage of fluorine with time. Obviously, in the presence of the ion beam, fluorine adatoms can be removed by "physical" sputtering. These sputtered adatoms may or may not leave the surface bonded to a Si substrate atom. Thus, we must be cautious in correlating removal of fluorine adatoms with removal (i.e., etching) of Si
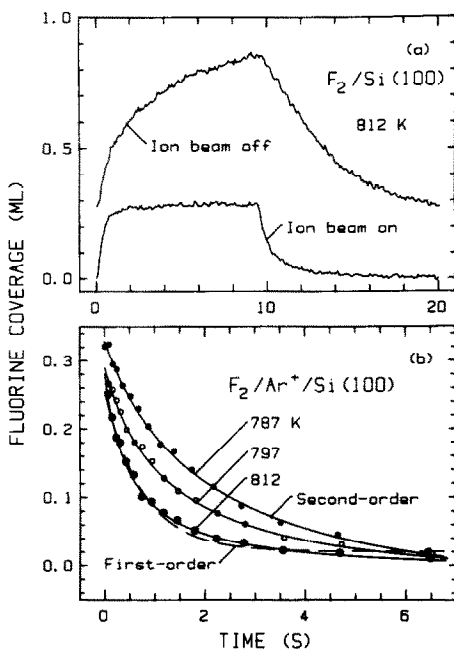
Fig. 20. (a) XPS waveforms produced by square-wave modulating the incident F_2 flux and monitoring simultaneously the fluorine coverage via XPS both in the absence of the ion beam and in the presence of a coincident Ar^+ ion beam (1.5 keV, approximately 8 μA cm^{-2}). Note that the presence of the ion beam leads to both a smaller steady-state coverage and a more rapid rate of depletion of the coverage of fluorine in the F_2 beam off region. (b) Isothermal decomposition of the silicon-fluoride adlayer at three different substrate temperatures and in the presence of the coincident Ar^+ ion beam. These curves were derived from waveforms such as that shown in (a). The solid curves represent analytic fits to second-order decomposition kinetics. The experimental uncertainties are indicated by the size of the plotted symbols.

substrate atoms. Since "physical sputtering" is expected to depend weakly on the substrate temperature, whereas the so-called "chemical sputtering" [6] may exhibit a temperature dependence, the effect of varying the surface temperature should be decisive in assessing the relative importance of purely "physical sputtering" in these experiments.

A representative set of experiments, where the ion beam was either off or on, is depicted in fig. 20a where the fluorine coverage is plotted versus time. The square-wave modulated F_2 flux was the same in both cases, the "on" flux estimated to be ~ 2–3 ML s^{-1}. The Ar^+ ion current collected by the sample was kept constant at 4 μA, which for our beam spot size of ~ 0.5 cm^2 corresponds to a flux of 5×10^{13} ions cm^{-2} s^{-1} (or 0.074 ML s^{-1}). As may be seen in fig. 20a, the presence of the ion beam produces two effects: the apparent steady-state coverage is reduced (i.e., $\theta_{F,s} \approx 0.9$ ML for Ar^+ beam
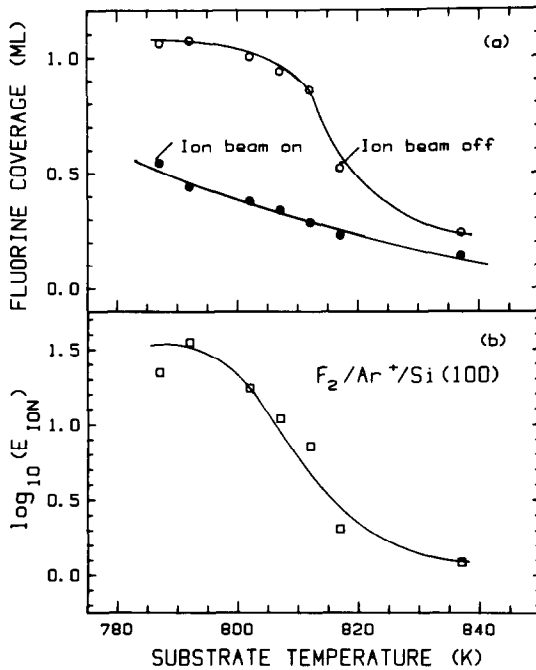
Fig. 21. (a) Steady-state fluorine coverage both in the presence and absence of the 1.5 keV Ar$^+$ ion beam as a function of the substrate temperature. (b) The calculated ion-enhancement factor, E_{ion}, as a function of the substrate temperature, derived from the measured steady-state coverages given in (a). E_{ion} represents a maximum enhancement factor for acceleration of the substrate removal reaction due to the ion beam (see text).

off, $\simeq 0.3$ ML for Ar$^+$ beam on); and the relative "response rate" appears to be greater with the ion beam on. Both of these observations suggest that the rate of removal of the fluorine adatoms is accelerated by the ion beam. We shall consider these two effects separately.

The variation of the steady-state fluorine coverage with both the substrate temperature and the presence of the ion beam is shown in fig. 21a. In all cases, a lower coverage is observed with the ion beam on, which implies that the rate of removal of fluorine adatoms is increased by the ion beam. That is, if the probability of adsorption of F$_2$ is unaffected by the presence of the ion beam, then for equal fluxes of F$_2$ a lower steady-state coverage results in a higher rate of adsorption, and thus a higher rate of desorption and/or decomposition. It is also important to note that, in both cases, i.e., ion beam either on or off, the steady-state coverage decreases with increasing substrate temperature. As discussed above in section 3.2.3, this implies that the rate of reaction and/or process leading to the removal of fluorine adatoms increases with temperature. Since this occurs in the presence of the ion beam, these data

suggest that the kinetics describing the $F_2/Si(100)$ interaction in the presence of the ion beam are temperature dependent. Note, however, that the relative difference between the steady-state coverages in each case decreases with increasing surface temperature.

The apparent ion-enhancement of the $F_2/Si(100)$ reaction can be quantified if we assume that the initial probability of adsorption is unaffected by the ion beam, and employ eq. (1) to account for the coverage dependence of the adsorption kinetics, viz. $r_{des} = r_{ads} = S_0 F_{F_2}(1 - \theta_F/\theta_{sat})^2$. In particular, we define an ion-enhancement factor, E_{ion}, given by $E_{ion} = (1 - \theta_F/\theta_{sat})^2_{ON}/(1 - \theta_F/\theta_{sat})^2_{OFF}$. Since we cannot exclude "physical sputtering" of the fluorine adatoms, this value represents a maximum for ion-enhancement of the Si substrate removal reaction. The values calculated for the apparent ion-enhancement factor, E_{ion}, are displayed in fig. 21b as a function of the substrate temperature. Due to the sensitivity of E_{ion} to the value assigned for the saturation coverage (we employed $\theta_{sat} = 1.2$ ML, which was found for $T_s = 600$ K), especially at the lower temperatures (i.e., large E_{ion}), the quantitative significance of these values should be viewed with caution. We see that the apparent enhancement factor is quite large at the lower temperatures, i.e., ~ 20–30, but decreases to nearly unity at 840 K.

The kinetics of the reaction leading to the removal of fluorine adatoms from the Si surface in the presence of the ion beam was evaluated by analyzing coverage versus time curves, such as those shown in fig. 20a, considering only the depletion (i.e., F_2 beam off) regime. These data are displayed in fig. 20b. The decomposition kinetics were assumed to take the form $-d\theta/dt = k_{d,n}\theta^n$, and only coverages ≤ 0.3 ML were considered in the nonlinear least-squares fits. This latter procedure was adopted primarily due to the observation here of zero-order kinetics for the thermal reaction for $\theta_F \geq 0.3$ ML (see sections 3.2.1–3.2.3). As may be seen in fig. 20b, the data were best described by assuming that the kinetics were second-order, i.e., $n = 2$. Second-order kinetics is consistent with that derived in section 3.2.3 for the low coverage regime in the absence of the ion beam. It is important to note that, for the submonolayer regime, the reaction order for a "physical sputtering" mechanism is expected to be first-order in the coverage of fluorine [61]. Therefore, the observation of second-order kinetics seems to suggest that the ion-enhanced "reaction" does not simply involve the sputtering of fluorine adatoms and/or SiF_x species, rather, it may hold more similarities to the thermal reaction examined here. The relative importance of physical sputtering may be discounted also based on the implied sputter yields. We estimate that the maximum rate of removal of fluorine adatoms in the presence of the ion beam was approximately 1 ML s^{-1}, which implies a sputter yield as great as 14 F atoms/Ar$^+$ ion. This value appears to be too large to be solely accounted for by physical sputtering alone [61].

A kinetic analysis suggests also the importance of a reaction mechanism
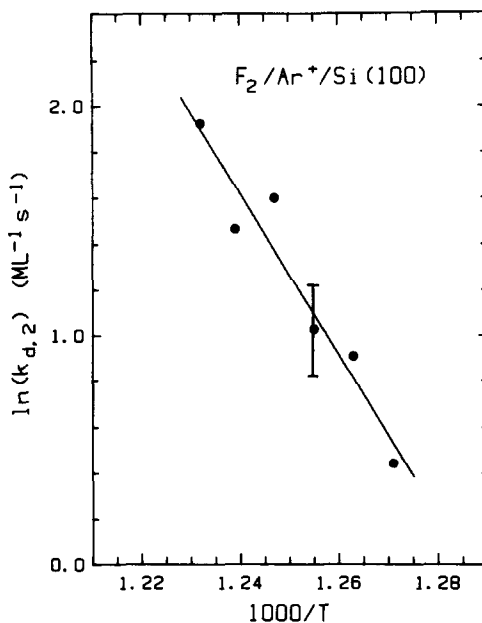
Fig. 22. Arrhenius plot of the second-order reaction rate coefficient derived from the analytic fits displayed in fig. 20b for the data obtained in the presence of the coincident Ar$^+$ ion beam.

that is not based on physical sputtering. The values of the second-order rate coefficient, $k_{d,2}$, derived from the fits displayed in fig. 20b, are displayed as a function of the reciprocal temperature in fig. 22. In order to avoid a superposition of effects due to the purely thermal reaction and those due to the ion-enhanced reaction, we consider only those data for which the apparent ion-enhancement is quite large, i.e., $E_{ion} \geq 10$ or $T_s \leq 812$ K. As may be seen, the fit to an Arrhenius expression is reasonable. From these data, we derive an activation energy equal to 70 ± 10 kcal mol^{-1}, and a second-order preexponential factor equal to $3.8 \times 10^{19 \pm 3}$ ML^{-1} s^{-1}, or $5.6 \times 10^{4 \pm 3}$ cm^2 s^{-1}. Note the similarity between these values and those derived above in section 3.2.3 for the thermal reaction, where the activation energy was equal to 59 ± 5 kcal mol^{-1}, and the second-order preexponential factor was given by 1.7×10^3 cm^2 s^{-1}.

As a final consistency check, the data obtained for the Ar$^+$ beam off cases were analyzed also. It was found that for $T_s \geq 817$ K and $\theta_F \leq 0.3$ ML, the depletion regimes were described best by second-order kinetics. Moreover, a comparison of the second-order rate coefficients derived for the Ar$^+$ beam off cases to those found for the Ar$^+$ beam on cases *for which the steady-state coverage was nearly the same* [e.g., beam on ($T_s = 787$ K) and beam off ($T_s = 817$ K), cf. fig. 21b] found agreement within a factor of 2. Thus, the

agreement between both the steady-state coverages and the rate coefficients suggests that the ion beam does not directly affect the kinetics of adsorption of F_2.

4. Discussion

4.1. Adsorption kinetics

Considerable recent experimental work has focused on employing molecular beam techniques to investigate the mechanisms involved in the dissociative adsorption of diatomic molecules (homo- and heteronuclear) on a variety of solid surfaces. In general, the dominant mechanisms have been found to involve either a "direct" reaction of the molecule with the surface, for which the translation energy of the incident gas phase molecule plays a key role, or dissociative adsorption via a (molecular) precursor state, for which the substrate temperature is most important. In the former cases, by increasing the incident translation energy of gas phase molecules, a dramatic increase in the probability of adsorption has often been observed. On the other hand, in the latter case, the initial probability of adsorption is most often sensitive to the substrate temperature. In addition, trapping into molecular adsorption sites lying above filled (dissociative) adsorption sites can lead to an adsorption probability which is only weakly dependent on coverage. Finally, depending on the experimental conditions chosen, in certain cases *both* mechanisms have been found to play significant roles concerning the adsorption kinetics of a single adsorbate/substrate system [48].

A discussion of our results concerning the adsorption of F_2 on the Si(100) surface will be aided by the one-dimensional potential energy diagram displayed in fig. 23. Here we designate the gas phase molecule $F_2(g)$, the dissociative state $F(a)$ representing fluorine adatoms, and the two possible precursors – the intrinsic state $F_2^*(a)$ lying over an empty adsorption site or sites, and the extrinsic state $F_2'(a)$ lying over a filled adsorption site or sites. Since we consider here the dissociative adsorption of F_2, these precursor states can be expected to be represented by molecularly adsorbed F_2. Due to the complexity of the F_2/Si(100) adsorption system at high coverages, e.g., lattice penetration by fluorine, multiple binding states, etc., this diagram can only be meaningfully applied to coverages of ~ 1 ML and below. Note that, to facilitate the presentation, the binding energies of the precursor states implied by fig. 23 have been greatly exaggerated.

Based on the results given in section 3.1.2, the dissociative adsorption of F_2 on the clean Si(100) surface is a relatively facile reaction. In particular, we found that the initial probability of adsorption was equal to 0.46 ± 0.02, independent of both substrate temperatures between 120 and 600 K, and
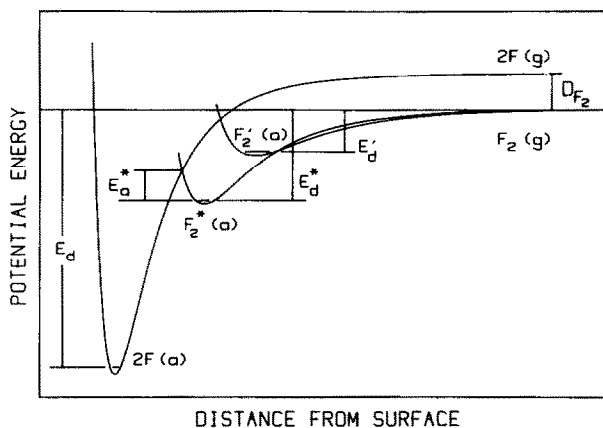
DISTANCE FROM SURFACE

Fig. 23. One-dimensional potential energy diagram representing the F_2/Si(100) system. $F_2'(a)$ is the extrinsic precursor lying over a filled adsorption site or sites, and $F_2^*(a)$ is the intrinsic precursor, lying over an empty site. The implied binding energies of the precursor states relative to the dissociative state F(a) have been greatly exaggerated to facilitate the presentation.

incident translational energies of the F_2 molecules between 1.5 and 19 kcal mol^{-1}. We shall assume for the moment that an intrinsic precursor state exists. Making this assumption, two possibilities exist that would be consistent with the experimental observations: (i) trapping into the intrinsic precursor state is inefficient under the experimental conditions considered here; and (ii) trapping is efficient, with the rate of (dissociative) chemisorption relative to desorption from the precursor state being essentially independent of substrate temperature between 120 and 600 K. Concerning the first possibility, in the absence of efficient trapping into the intrinsic precursor state, the adsorption reaction would be expected to exhibit the characteristics of a "direct" surface reaction, i.e., display little or no dependence on the substrate temperature. Provided adsorption is also unactivated, this explanation would be consistent with the observed lack of dependence on the incident translational energy. Concerning the second possibility, a weak dependence on substrate temperature implies one of the following situations: (a) the activation energies E_a^* and E_d^* are approximately equal; or (b) the activation energy associated with conversion from the intrinsic precursor state to the dissociative state (E_a^*) is much less than the activation energy of desorption from the intrinsic precursor state (E_d^*). In case (a), i.e., $E_a^* \simeq E_d^*$, the probability of adsorption will essentially be independent of temperature at high temperatures, with a temperature dependence only becoming apparent at very low temperatures such that $T_s \leq |E_d^* - E_a^*|/k_B$ [62]. In case (b), i.e., $E_a^* \ll E_d^*$, the probability of adsorption will be independent of temperature at low temperatures, and only when $T_s \geq E_d^*/k_B$ will the adsorption probability begin to decrease with

increasing temperature. Depending upon the absolute values for the trapping probability into the intrinsic precursor state, and the preexponential factors associated with chemisorption ($k_a^{*(0)}$) and desorption ($k_d^{*(0)}$) from the precursor state, either case (a) or (b) would be consistent with the absolute value for the initial probability of adsorption measured here, i.e., 0.46.

Clues as to the presence and importance of an intrinsic precursor state would be best addressed by an additional set of experiments. In particular, it would be desirable to cool the Si surface to much lower temperatures than were examined here, e.g., near 20 K, in order to possibly "freeze-in" the intrinsic precursor state, verifying its presence by an appropriate surface-sensitive spectroscopy [37,62]. Alternatively, by examining the scattered F_2 flux as a function of takeoff angle and surface temperature it may be possible to detect a trapping/desorption channel [32], which would be associated with the precursor state. Obviously until such experiments are conducted, based on our results it is difficult to comment meaningfully on the possible presence and relative stability of an intrinsic precursor state for F_2 adsorbed on the Si(100) surface. Nonetheless, for the experimental conditions examined here, its influence on the kinetics of adsorption appears to be negligible.

Unlike the somewhat ambiguous situation concerning the adsorption kinetics in the limit of zero-coverage, our results definitely point to the importance of a (mobile) extrinsic precursor state. In particular, at a substrate temperature of 120 K the probability of adsorption was found to be nearly independent of coverage for a large range. We were able to fit the coverage versus exposure curves to a model expression that included as a parameter the relative rates of desorption and migration from the extrinsic precursor. In particular, this parameter is defined as $K' = k'_d/k'_m$. Thus, an Arrhenius plot of K' versus reciprocal temperature will yield the difference of the activation energies, $E'_d - E'_m$, and the ratio of the preexponential factors $k'^{(0)}_d/k'^{(0)}_m$. An Arrhenius plot of the parameter k' obtained at 120, 200 and 300 K is displayed in fig. 24. Each of these values is the mean value obtained from two separate experiments. We see that the data are well described by an Arrhenius expression. From a fit of the data we obtain values for the kinetic parameters of $E'_d - E'_m = 1.1 \pm 0.3$ kcal mol^{-1} and $k'^{(0)}_d/k'^{(0)}_m = 10^{1.2 \pm 0.4} \simeq 17$. These values are quite reasonable, e.g., they compare well with values employed in time-dependent Monte Carlo simulations of precursor-mediated adsorption kinetics [63]. As expected, the activation energy for desorption from the extrinsic precursor exceeds that for migration. In addition, since desorption is associated with motion normal to the surface (i.e., characterized by a stretching frequency), whereas migration is associated with motion parallel to the surface (i.e., characterized by a frustrated translation), one expects the ratio of the preexponential factors to well exceed unity.

Another experimental observation suggests also the importance of the extrinsic precursor state to the kinetics of adsorption. In particular, the
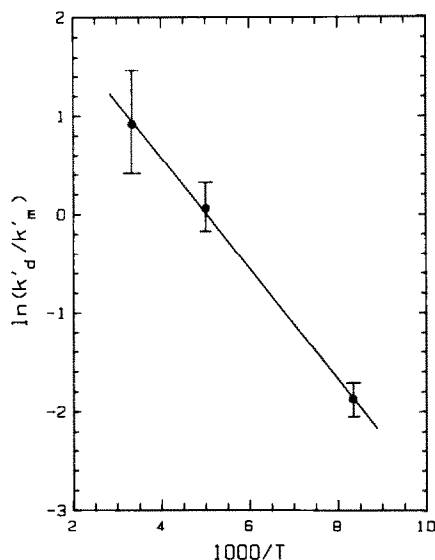
Fig. 24. Arrhenius plot of the parameter $K' \equiv k'_d/k'_m$ defined as the ratio of the rate coefficients for desorption and migration from the extrinsic precursor [see text and eq. (2)].

"saturation" coverage of the rapid adsorption phase determined from the fits displayed above in fig. 2 has been found to decrease with increasing temperature. For example, θ_s is 1.57 ML at 120 K, it decreases to 1.44 ML at 300 K, and finally to 1.18 ML at 600 K. It is important to note that this is not merely an artifact due to the lessened thermal stability of the adlayer above coverages of 1 ML. For example, as may be seen from the data shown in fig. 6, coverages up to ~ 1.7 ML are stable to 600 K. The decrease in the "saturation" coverage with increasing substrate temperature is most probably a manifestation of a decreased residence time in the extrinsic precursor state. Thus, at lower substrate temperatures, the residence time is increased, more sites may be accessed and the apparent saturation coverage is larger. Presumably, at significantly higher pressures (i.e., greater than 1 Torr) this reaction channel for the dissociative adsorption of F_2 above coverages of ~ 1.2 ML becomes important even at substrate temperatures well above 200 K. Since high coverages of fluorine ($\geq$ 5–6 ML) are necessary to produce a significant rate of decomposition for temperatures of 400 K and below (cf. figs. 6 and 7), these observations should be kept in mind when modeling the steady-state etching of Si by F_2.

Our results concerning the effects of the translational energy of the incident F_2 molecules on the adsorption probability by no means represent an exhaustive study. Specifically, our results are representative of a single substrate temperature (120 K) and a single, relatively glancing angle of incidence (75°

from normal). Consequently, drawing broad conclusions from these data is probably unwise. Two aspects of the adsorption kinetics warrant discussion, namely, the effect of $\langle E_{tr} \rangle$ on both the initial probability of adsorption, and the probability of adsorption above coverages of ~ 1.5 ML, i.e., the "slow" phase of adsorption (cf. fig. 1). Within experimental uncertainties, the initial probability of adsorption of F_2 remained constant as $\langle E_{tr} \rangle$ was increased from 1.5 to 19 kcal mol^{-1}. Since $S_0 = 0.46$ for the 10%F_2/Ar mixtures ($\langle E_{tr} \rangle = 1.5$ kcal mol^{-1}), the adsorption reaction in the zero-coverage limit is relatively facile. On the other hand, some effect due to $\langle E_{tr} \rangle$ of the incident F_2 molecules might be expected for the higher coverage regime. For example, Rettner et al. [48], examining the dissociative adsorption of O_2 on the W(110) surface, found that higher coverages could be obtained with a higher energy reactant beam. For the two gas mixtures considered here, we have found no evidence for such an effect for the F_2/Si(100) system. It is possible that at translational energies higher than those considered here, where $\langle E_{tr} \rangle \leq 19$ kcal mol^{-1}, some increase in the adsorption probability at high coverages may be observed. However, we feel this is unlikely due to the above discussed importance at high coverages of a reaction channel mediated by an extrinsic precursor.

The results obtained with the partially dissociated F/F_2 beams are qualitatively consistent with those reported by Stinespring et al. [24]. We estimate that the adsorption probability of atomic fluorine on the clean Si(100) surface is equal to 0.5 ± 0.3, i.e., very similar to the value found for molecular fluorine. On the other hand, clear differences were observed for the "slow" adsorption phase, indicative of coverages ≥ 2 ML, with the adsorption probability for F(g) greatly exceeding that for F_2(g). For example, for a coverage of 3–4 ML, the adsorption probability of F(g) exceeds that for F_2(g) by a factor of ~ 200, the calculated value for F(g) equal to 0.28 ± 0.1 for this coverage regime. It is of interest to note that this value is comparable to that obtained for the initial probability, i.e., 0.5 ± 0.3, which suggests that the adsorption probability of atomic fluorine is only weakly dependent on coverage for this coverage regime and $T_s = 120$ K. On the other hand, apparently unlike molecular fluorine, the adsorption of atomic fluorine at coverages above 2 ML may be activated, as evidenced by the data displayed in fig. 4. Clearly, concerning this last observation, a more complete data set concerning the effect of $\langle E_{tr} \rangle$ on the adsorption of F(g) on Si, especially at high coverages, is most desirable.

4.2. Decomposition / desorption kinetics

A discussion of our results concerning the kinetics of the reactions between F_2(g) and the Si(100) surface that lead to the gasification of the substrate may be conveniently divided into three separate issues: (i) the qualitative aspects of the decomposition reaction, including the product yields, the thermal stability

of the adlayer, etc.; (ii) the kinetics of decomposition in the monolayer regime; and (iii) the kinetics of $SiF_2(g)$ formation in the limit of very low fluorine adatom coverages. Our results involving the steady-state thermal decomposition reaction will be discussed with a particular emphasis on the implications of these results in regard to the mechanism of the "high" pressure etching reaction between $F_2(g)$ and the Si substrate.

The major features of the thermal decomposition of silicon-fluoride adlayers, representing fluorine coverages from 0.5 to ~ 13 ML, are summarized well by the data shown above in figs. 6–8. Briefly, we have found that for initial coverages below ~ 3 ML, SiF_2 is the *major* gas phase reaction product. Above a coverage of ~ 3 ML, the relative yield of $SiF_2(g)$ remained essentially constant, whereas that for $SiF_4(g)$ increased continuously. These are the *only* reaction products observed, i.e., the radicals $SiF(g)$ and $SiF_3(g)$ were not observed, nor was $Si_2F_6(g)$. The simple explanation for the observed product distributions is that at higher fluorine coverages the relative proportion of more highly fluorinated intermediates, such as $SiF_3(a)$ [10,17], is greater, and, consequently, formation of the more thermodynamically stable product, $SiF_4(g)$, dominates. This influence of the fluorine coverage on the product distribution has been pointed out previously by Winters and Coburn [16]. In particular, they reported that the production of $SiF_2(g)$ increased with decreasing coverage.

The relative thermal stabilities of the silicon-fluoride adlayers examined here can be separated into three groups. Coverages below ~ 2 ML are stable to ~ 600 K, with $SiF_2(g)$ being the major reaction product in this regime. Coverages below ~ 6 ML are stable to nearly 400 K, the two-peaked $SiF_4(g)$ desorption feature occurring between 400 and 800 K [cf. fig. 7a] being the dominant new feature for this coverage regime. Finally, for coverages between ~ 6 and 13 ML, the adlayer is not stable even below 200 K, where $SiF_4(g)$ is the dominant reaction product. Presumably, this coverage regime is quite similar to those examined under "realistic" etching conditions, such as those employing XeF_2 [17].

The most intriguing aspect of our investigation of the decomposition kinetics undoubtedly involves the complex behavior observed in the monolayer regime, e.g., for initial coverages of 1–1.3 ML the observation of zero-order kinetics for $\theta_F \approx 0.3$–1.0 ML [38]. Two experimental observations suggest strongly that arguments based on a thermodynamically driven domain formation (i.e., due to adatom–adatom interactions) [60] are not relevant in this case. In particular, we have observed the following: (i) the kinetics of the decomposition reaction are dependent on the *initial* coverage of fluorine adatoms [cf. figs. 9b, 10b and 11b]; and (ii) the spatial inhomogeneity of the decomposition reaction [38] is due to the kinetics of the reaction, not a thermodynamically driven phase segregation (cf. fig. 18). Thus, any mechanistic model proposed must be consistent with these two observations.
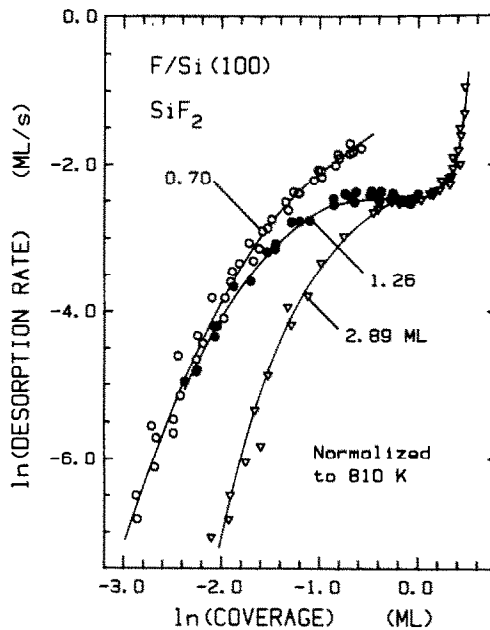
Fig. 25. "Order plot" of the (ln) rate of SiF$_2$ desorption versus the (ln) coverage of fluorine adatoms for three different initial coverages. These data were derived from those displayed in figs. 9b, 10b and 11b and were normalized to a common temperature of 810 K.

The dependence of the decomposition kinetics on the initial coverage of fluorine adatoms is portrayed in fig. 25. Here we have replotted the data from the "order plots" given in figs. 9b, 10b and 11b by normalizing the data to a single substrate temperature of 810 K. The normalization procedure made use of the measured activation energies given in fig. 12. The dependence on the initial coverage of fluorine adatoms is quite striking. We believe the most plausible explanation for these results involves preferential reactivity at surface defects such as atomic steps. We shall attempt to justify this proposition in the following discussion.

Before discussing in detail the variation of the reaction kinetics with the adlayer composition and/or configuration, it is useful to consider possible explanations for preferential reactivity at surface defects. A relatively simple explanation is preferential formation of the appropriate adsorbed intermediate at defect sites, e.g., a SiF$_2$(a) species. [Note that, by SiF$_x$(a) species, we mean x fluorine atoms are coordinated to a single Si surface atom.] For example, McFeely and co-workers [10] have demonstrated that SiF(a) is the dominant species in the monolayer regime on a Si(100) surface. They suggest that it is the *only* one on a perfect (100) surface, with the SiF$_2$(a) and SiF$_3$(a) species confined to defect sites on a imperfect (real) surface. The latter is most

probably a manifestation of a reduced degree of coordinative saturation of the Si surface atoms at a step. Thus, since formation of $SiF_2(g)$ almost certainly proceeds through a $SiF_2(a)$ species, preferential formation of this intermediate at defect sites provides a convenient explanation for enhanced reactivity.

As may be seen in fig. 25, for an initial coverage of 0.70 ML, the apparent order of reaction is positive for all coverages, decreasing in magnitude with increasing coverage. It is important to note that this coverage is approximately one-half of the "saturation" value for the "fast" adsorption phase. If the decomposition reaction involves the formation of $SiF_2(a)$ species at defect sites, an important parameter is the *local* coverage of fluorine in the vicinity defect sites. Since we have observed second-order Langmuirian adsorption kinetics ($T \geq 300$ K), the adlayer configuration below saturation is expected to be represented by a uniform distribution of fluorine adatoms. Thus, initially, this local coverage is well approximated by the mean coverage. Depending upon the mobility of fluorine adatoms and the relative thermodynamic stability of the adsorbed species, i.e., $SiF(a)$ versus $SiF_2(a)$ species, this local coverage may or may not vary as the decomposition proceeds. In particular, if the defect sites do not remain saturated, i.e., fully fluorinated, as the decomposition proceeds then a positive reaction order in the coverage of fluorine is expected.

The situation is considerably different for an initial coverage of 1.3 ML, i.e., near saturation of the "fast" adsorption phase. For this initial coverage, we have observed positive-order kinetics below ~ 0.3 ML, and zero-order kinetics between ~ 0.3 and 1.0 ML. At this initial coverage it may be reasonably assumed that all Si dangling bonds have been coordinated to fluorine atoms and that the adlayer consists of primarily $SiF(a)$ species with $SiF_2(a)$ [and possibly $SiF_3(a)$] species populating defect sites. It is important to note that a significant fraction (e.g., 5–10%) of defect sites (steps, vacancies, Si "adatoms", "missing dimers") can be expected to be present on a typically prepared clean Si(100) surface [64]. Thus, since these defect sites are intrinsic to the surface, the model does not imply an acceleratory region in the rate of decomposition, e.g., due to nucleation about a point defect. As may be seen in fig. 13, no acceleratory region was observed.

In regards to sustaining the zero-order kinetics for an initial coverage of 1–1.3 ML, since the decomposition reaction leads to substrate removal, defect sites such as atomic steps are regenerated. If the number these defect sites remains constant as the reaction proceeds, e.g., due to preferential orientation of the steps along crystallographic directions [65] or a sufficiently rough step boundary that does not increase in "area", then the reaction will also exhibit zero-order kinetics. Concerning the spatial inhomogeneity of the decomposition, provided fluorine adatoms do not diffuse into "open" areas of the Si substrate, the decomposition will proceed via a moving defect boundary (e.g.,

atomic step) that "consumes" fluorine adatoms as the reaction progress. Thus, in this scenario, there is a coincidence of defect sites and domain boundaries.

For an initial coverage of 2.89 ML, the coverage dependence is quite complex. In particular, positive-order kinetics are observed below ~ 0.6 ML, zero-order kinetics are operative between 0.6 and 1.2 ML, and large positive order kinetics (approaching a reaction order of 10) are observed above ~ 1.2 ML. In keeping with our model for the decomposition reaction, the composition and configuration of the adlayer are undoubtedly responsible for this complicated behavior. Unlike the situation for initial coverages below saturation of the "fast" adsorption phase, it is very probable that the adsorption of ~ 3 ML of fluorine adatoms is accompanied by disruption of the Si substrate lattice. That is, due to insertion of fluorine atoms into Si–Si bonds with subsequent formation of a covalent Si–F bond, the registry of the lattice is disturbed and defect sites are actually *created* by the chemisorption of fluorine atoms.

We can develop a simple mathematical model to describe this situation. Let us assume that the clean Si surface contains a fraction of surface sites δ, where $\delta \ll 1$, for which $SiF_2(a)$ formation is facile and occurs during the "fast" adsorption phase. Let us assume further that for each fluorine atom chemisorbed above the saturation coverage of the "fast" adsorption phase, $\theta_{F,sat}$, a $SiF_2(a)$ species is created. Thus, for coverages above saturation of the fast adsorption phase, i.e., $\theta_F/\theta_{F,sat} > 1$, the coverage of $SiF_2(a)$ species predicted by this model will be given by $\theta_{SiF_2} = \delta + (\theta_F/\theta_{F,sat} - 1)$. If we assume that the order of the decomposition reaction is first-order in the coverage of $SiF_2(a)$ species, then this expression predicts that the reaction order of the decomposition reaction in the total coverage of fluorine adatoms, θ_F, for $\theta_F > \theta_{F,sat}$ will be given by

$$\frac{\partial \ln(k_d \theta_{SiF_2})}{\partial \ln \theta_F} = \frac{\theta_F/\theta_{F,sat}}{\delta + (\theta_F/\theta_{F,sat} - 1)}.$$

Note that the above expression predicts that the apparent reaction order for $\theta_F \simeq \theta_{F,sat}$ will be given by $1/\delta$, i.e., $\gg 1$. Thus, the large apparent reaction orders observed for coverages above ~ 1.2 ML can be explained by this model.

This mechanism is consistent also with the observed break in the order of the kinetics at 0.6 ML for an initial coverage of 2.89 ML, i.e., the transition from zero-order kinetics to positive-order kinetics with decreasing coverages. In particular, the deviation from zero-order kinetics can be expected to scale with the concentration of defect sites where $SiF_2(a)$ species may form. For example, at an initial coverage of 1.3 ML, the break is apparent at ~ 0.3 ML, which suggests a defect site density on the order of 15% (i.e., $2F(a) \rightarrow SiF_2(a)$). On the other hand, for an initial coverage of 2.89 ML, the break occurs at 0.6

ML, which suggests that the defect site density is greater in this case. Thus, the more limited coverage range for which zero-order kinetics apply observed for an initial coverage of 2.89 ML is consistent with Si lattice disruption at high coverages.

In concluding the discussion of the experimental results portrayed in fig. 25 we have been able to obtain a qualitative picture of the decomposition reaction by employing a relatively simple mechanistic model, i.e., preferential formation of $SiF_2(a)$ species at defect sites. Namely, for initial coverages below saturation of the fast adsorption phase, these defect sites are and remain unsaturated, and the decomposition reaction exhibits positive order kinetics. For an initially saturated adlayer, the defect sites are saturated, and remain so by continually drawing on a reservoir of nearest neighbor fluorine adatoms, i.e., via a moving domain boundary between regions of a locally saturated adlayer and clean surface. This results in the observation of zero-order kinetics over a large coverage range. At high coverages defect sites are created by the chemisorption of fluorine atoms and, consequently, the decomposition reaction exhibits a large positive order above coverages near "saturation". It must be stressed that, in the absence of additional experimental results, extrapolation of this mechanism to significantly different reaction conditions (e.g., temperatures) may be both difficult and unwise. For example, this simple model does not explicitly address the crucial effects of fluorine adatom mobility, in addition to the relative thermodynamic stabilities of the adsorbed species, i.e., $SiF(a)$ and $SiF_2(a)$.

At this point it is useful to consider explicitly a quantitative kinetic model for the decomposition reaction leading to the desorption of SiF_2. The proposed overall mechanism is given by

$$F(a) + SiF(a) \underset{k_{-1}}{\overset{k_1}{\rightleftharpoons}} SiF_2(a) \tag{6}$$

and

$$SiF_2(a) \overset{k_d}{\rightarrow} SiF_2(g). \tag{7}$$

In eq. (6), F(a) represents either a nearest neighbor SiF(a) species or a diffusing and/or "interstitial" [27] fluorine atom. The reaction mechanism embodied by eqs. (6) and (7) is deceptively simple. Although the reaction given by eq. (7) is almost certainly first-order in θ_{SiF_2}, the formulation of the kinetics given by eq. (6) is considerably more complicated. The difficulty in describing the reactions of eq. (6) lies in accounting for both the effects of adlayer configuration and/or mobility (i.e., homogeneous versus inhomogeneous), and the effects of defects. The latter aspects is crucial since, as discussed above, the work of McFeely et al. [10] implies that $SiF_2(a)$ formation is restricted to defects at low coverages. To simplify matters, we shall assume that the

forward reaction of eq. (6) has some general coverage dependence, $g(\theta_F)$, and that the reverse reaction is first-order in the coverage of $SiF_2(a)$ and first-order in the fraction of vacant sites, i.e., $(1 - \theta_F/\theta_{F,sat})$, assuming $\theta_F \gg \theta_{SiF_2}$. If we make a pseudo-steady-state approximation on the coverage of $SiF_2(a)$ (i.e., $d\theta_{SiF_2}/dt = 0$) we obtain the following for the rate of desorption of SiF_2:

$$r_{d,SiF_2} = k_d \theta_{SiF_2} = k_d \left[\frac{K_1}{(k_d/k_{-1}) + (1 - \theta_F/\theta_{F,sat})} \right] g(\theta_F), \qquad (8)$$

where $K_1 = k_1/k_{-1}$. Two limits of eq. (8) are of interest. If the reaction is desorption rate-limited, i.e., $k_d \ll k_{-1}(1 - \theta_F/\theta_{F,sat})$, eq. (8) reduces to $r_{d,SiF_2} \simeq k_d K_1 g(\theta_F)/(1 - \theta_F/\theta_{F,sat})$, whereas if the reaction is limited by the rate of formation of $SiF_2(a)$ ("reaction-limited"), i.e., $k_d \gg k_{-1}(1 - \theta_F/\theta_{F,sat})$, then $r_{d,SiF_2} \simeq k_1 g(\theta_F)$.

Given the kinetic model embodied by eq. (8), a reasonable mechanism for the zero-order regime can be put forward. In particular, we propose that in this regime the reaction is limited by the rate of SiF_2 desorption and, provided the coverage of fluorine adatoms is above some critical value, the concentration of the adsorbed $SiF_2(a)$ species remains saturated. In terms of the kinetic model, $K_1 g(\theta_F)/(1 - \theta_F/\theta_{F,sat}) \simeq \theta_{SiF_2,sat}$, for $\theta_F \geq \theta_{F,crit}$, and $r_{SiF_2} \simeq k_d \theta_{SiF_2,sat}$. Thus, the apparent zero-order rate coefficient is the product of a first-order coefficient, k_d, and a coverage, $\theta_{SiF_2,sat}$. A reasonable upper limit for $\theta_{SiF_2,sat}$ is 0.15 ML, i.e., $\frac{1}{2}$ of 0.3 ML, the lower boundary of the zero-order regime for initial coverages of 1.3 ML. Accounting for stoichiometry (i.e., $2F(a) \rightarrow SiF_2(g)$) this implies first-order preexponential factors for the desorption of SiF_2 of 4.7×10^{17} s^{-1} and 4.7×10^{22} s^{-1}, employing the values obtained via XPS and temperature-programmed desorption (TPD), respectively. The former value compares well to that predicted by transition state theory, provided the transition state $SiF_2^\dagger$ is assumed to possess considerable two-dimensional translational and rotational freedom [52,66]. However, the latter value is beyond any reasonable limit for a first-order preexponential factor.

A reasonable question to pose is are the XPS and TPD results consistent, e.g., might they actually reflect different mechanisms as a consequence of the (somewhat) different temperature ranges examined. Experimental data, obtained via the two techniques and representative of the zero-order regime, are displayed in fig. 26. The data from TPD represent an initial coverage of 1.26 ML, and seven different fixed coverages of 0.4, 0.5,...1.0 ML. An analysis of the TPD spectra gave kinetic parameters of $k_{d,0}^{(0)} \simeq 2 \times 10^{22}$ ML s^{-1} and $E_d \simeq 87 \pm 2$ kcal mol^{-1} for the zero-order regime. On the other hand, from the isothermal decomposition experiments employing XPS, we obtained kinetic parameters of 1.4×10^{17} ML s^{-1} and 68 ± 5 kcal mol^{-1} for this same coverage regime. It is important to note that the majority of the TPD results displayed in fig. 25 are confined to the temperature range of 780–805 K. Note also that the experimental uncertainty in the rates derived from TPD increase with
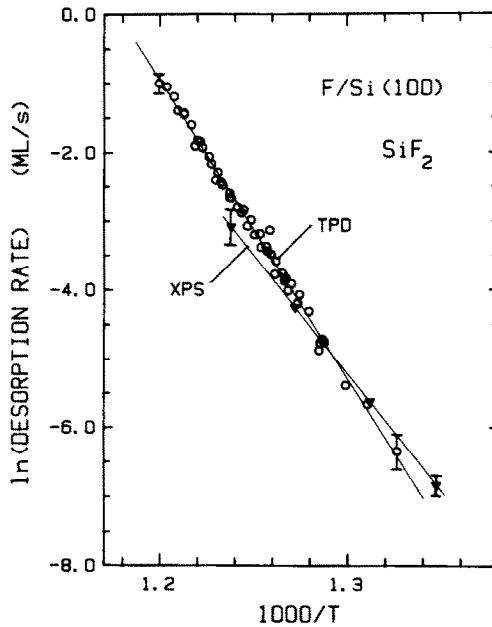
Fig. 26. Arrhenius plot of the rate of SiF$_2$ desorption versus the reciprocal temperature. These data are representative of the zero-order regime and were obtained via TPD (open circles) and XPS (closed triangles).

decreasing temperature (i.e., decreasing rate), whereas those from XPS *decrease* with decreasing temperature, due primarily to the need for a nearly step-function change in the temperature at the higher substrate temperatures. Stated in another fashion, the uncertainties in the values obtained from each technique are greatest in the region where the two curves intersect (cf. estimated error bars in fig. 26). We shall consider separately two possibilities for this apparent discrepancy in the measured kinetic parameters – the first involving a physical explanation, and the second involving the possible role of experimental artifacts.

Bauer and co-workers [67], examining the desorption of submonolayer metal overlayers (Ni, Cu, Ag and Au) from the W(110) surface, found that Arrhenius plots of the rates of desorption (at a fixed coverage) were not linear, but could be described by two intersecting straight lines. These results were interpreted as due to a phase transition in the adlayer, with the high temperature, low activation energy and low preexponential factor regime characterized by desorption from a two-dimensional "vapor" phase, and the low temperature regime by desorption from a "condensed" phase. In these cases, due to attractive adatom–adatom interactions, the activation energy for desorption from the condensed phase was greater. Probably more relevant to the work

here on the F/Si(100) system are the observations that have been made recently concerning the desorption of H_2 from the Si(100) surface [68]. Namely, two linear Arrhenius regimes were found, with the high temperature regime exhibiting the higher activation energy and preexponential factor. In this case, the results can be interpreted by invoking parallel, competing reaction mechanisms, with one mechanism dominating in each regime. This physical explanation, i.e., parallel reaction mechanisms as opposed to adlayer phase segregation effects, is the more probable one concerning the data displayed here in fig. 26. In particular, as discussed above in section 3.2.4, we find no evidence for a thermodynamically driven phase segregation in the adlayer, rather, the observed inhomogeneity is due to the *kinetics* of the decomposition reaction.

Experimental artifacts that could lead to the apparent discrepancy displayed in fig. 26 include: (i) the presence of temperature gradients across the sample, which would produce an erroneous thermocouple reading; (ii) variations in the angular and/or velocity distribution of the desorbing $SiF_2(g)$ product with substrate temperature; and (iii) the presence of additional reaction products, e.g. $SiF_4(g)$, which could influence the XPS results since the depletion of fluorine adatom coverage is measured. Concerning point (i), temperature gradients would most likely be manifest in the TPD spectra at the high heating rates, e.g., underestimating the substrate temperature due to a thermal time lag between the sample area viewed by the detector and the thermocouple. If this were the case, we would expect a systematic deviation of the data produced by the higher heating rates. As may be assessed from the data shown in fig. 26, which were produced by employing seven different heating rates, we find no evidence for deviations at the higher heating rates. This observation is consistent with theoretical expectations for the magnitude of thermal gradients. In particular, based on the configuration of our sample and the thermocouple, we estimate conservatively that gradients, if present, do not exceed 5 K. Concerning point (ii), assuming a $T^{1/2}$ dependence for effects due to the velocity distribution of the desorbing $SiF_2(g)$ product, the resultant effect on the TPD data shown in fig. 26 would be a total difference of ~ 3% between the extrema, i.e. negligible. However, if the desorbing $SiF_2(g)$ product is not thermally accommodated by the surface, the temperature dependence of the velocity distribution could be much stronger than $T^{1/2}$. If this was the case, the effect on the TPD data could be significant, i.e., much larger than 3%. Concerning point (iii), the presence of multiple reaction channels (i.e., reaction products) would invalidate the proportionality relationship $-d\theta_F/dt \propto r_{d,SiF_2}$. Depending on the predominance and energetics of the other [i.e., not $SiF_2(g)$] reaction channels, in general, the XPS and TPD results will differ. However, based on our calculations of the relative product yields (cf. fig. 8), for coverages below 2 ML the rate of production of $SiF_4(g)$ is at most 2% of that of $SiF_2(g)$. As discussed above in section 3.2.1, we were also able to

discount any significant production of SiF(g) and Si_2F_6(g). In addition, the ISS results presented in section 3.1.4 imply that diffusion of fluorine adatoms into the bulk, which would also lead to a depletion in the surface concentration of fluorine, is not significant. Thus, we conclude that it is unlikely the XPS results are not indicative of the desorption of SiF_2(g). Collecting our observations, and applying the appropriate experimental uncertainties, we estimate that the relative error in calculating the activation energies is ~ 5–10 kcal mol^{-1}, which may be compared to the measured difference between the two techniques of ~ 19 kcal mol^{-1}. Thus, we conclude that the physical explanations discussed above may be important in explaining the data depicted in fig. 26.

The kinetic model represented by eq. (8) may be employed also to suggest mechanisms for the decomposition reaction in the limit of zero coverage. As was demonstrated in section 3.2.3, in the low coverage limit the SiF_2(g) formation reaction is second-order in the coverage of fluorine adatoms. In terms of the kinetic model, in the limit of low coverages, the coverage dependence of the forward reaction of eq. (6) is most probably second-order, i.e., $g(\theta_F) \simeq \theta_F^2$. Thus, if the reaction is desorption-limited, $r_{d,SiF_2} \simeq k_d K_1 \theta_F^2$, whereas if it is formation-limited, $r_{d,SiF_2} \simeq k_1 \theta_F^2$, i.e., both mechanisms are consistent with second-order kinetics. Distinguishing between these two possibilities can be aided by knowledge of the coverages of the two intermediates under the reaction conditions considered in figs. 15 and 17. The concentration of SiF(a) species may be calculated by employing the steady-state rate of reaction ($S_0 F_0 \simeq 0.5$ ML s^{-1}) and the measured second-order rate coefficient ($k_{d,2}$). Similarly, the concentration of SiF_2(a) species may be calculated by employing the rate of reaction and the first-order rate coefficients for the desorption of SiF_2 implied by the data given by fig. 26. The results of these calculations, which correspond to the reaction conditions considered in figs. 15 and 17, are displayed in fig. 27. Unfortunately, due to the large spread in the coverages calculated for the SiF_2(a) species, which arises from the different kinetic parameters measured via XPS and TPD, we cannot explicitly identify which mechanism is operative under these reaction conditions. Note, however, that should the desorption-limited mechanism be the operative one, this will have important consequences on an interpretation of the measured apparent activation energy, which in this case is given by $E_{app} = E_d - E_{-1} + E_1$. In particular, employing $E_{app} = 59$ kcal mol^{-1} and $E_d = 68$–86 kcal mol^{-1} we find that $E_{-1} - E_1 = 9$–27 kcal mol^{-1}, which implies that the SiF_2(a) species is the more thermodynamically stable adsorbed species.

Equipped with the activation energy for desorption of SiF_2(a), implied by the XPS and TPD results, and if we assume that the equilibrium, $2F(a) \rightleftharpoons SiF_2(a) + Si(s)$, exists for those conditions examined via MMBRS, we are permitted a construction of a potential energy diagram for the reaction F_2(g) + Si(s) $\rightarrow$ SiF_2(g). This diagram is shown in fig. 28. The overall reaction
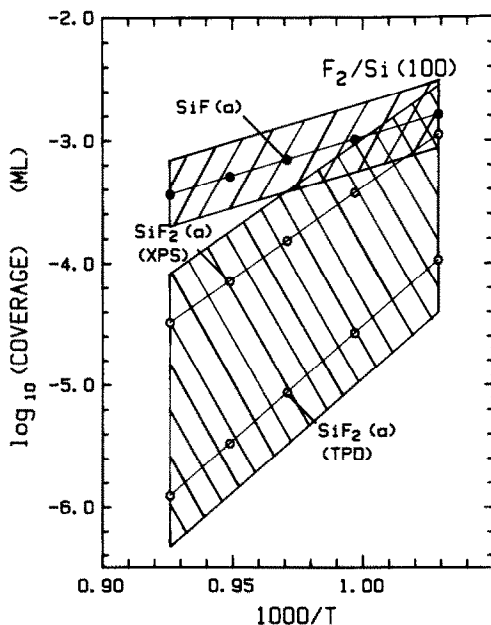
Fig. 27. Pseudo-steady-state coverages of the adsorbed SiF(a) and SiF_2(a) species calculated from the rate coefficients displayed in figs. 17 and 26, and corresponding to the reaction conditions of fig. 15. The hatched areas illustrate the experimental uncertainties involved in these calculations.

is exothermic by 141 kcal mol^{-1} [69]. The SiF_2(a) level may be set relative to the gas phase SiF_2(g) level by assuming a value for the activation energy of adsorption of SiF_2(g). A reasonable estimate is that this adsorption reaction is unactivated. From the MMBRS results, assuming that the pseudo-equilibrium, $2F(a) \rightleftharpoons SiF_2$(a) + Si(s), is maintained, the measured activation energy of 59 kcal mol^{-1} is equal to $E_1 - E_{-1} + E_d$, which sets the 2SiF(a) level with respect to SiF_2(g). (Note that if the reaction examined by MMBRS is formation-limited, $E_1 = 59$ kcal mol^{-1}, and we cannot specify the SiF(a) level with respect to the gas phase SiF_2(g) level.) It is of interest to compare the implied binding energy of an adsorbed fluorine adatom to those derived for gas phase SiF_x species, where $x = 1-4$. From fig. 28 the implied binding energy is $\frac{1}{2}(37 + 141 + 59) = 119 \pm 3$ kcal mol^{-1}. On the other hand, the average binding energy for the adsorbed fluorine adatoms associated with the SiF_2(a) species is $\frac{1}{2}(37 + 141 + (68-86)) = (123-132) \pm 3$ kcal mol^{-1}. Both of these implied binding energies compare well with the appropriate gas phase values. In particular, the bond dissociation energies for the gas phase species are equal to 123, 155, 135 and 160 kcal mol^{-1} for Si–F, SiF–F, SiF_2–F and SiF_3–F, which results in an average value for SiF_2 of $\frac{1}{2}(123 + 155) = 139$ kcal mol^{-1}. The agreement between the gas phase values and those implied in fig. 28 for the binding
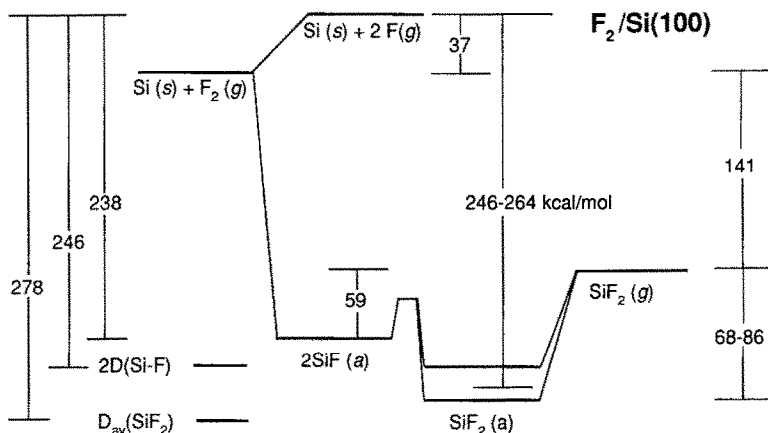
Fig. 28. Potential energy diagram illustrating the reaction between $F_2(g)$ and the substrate Si(s) that produces the gas phase reaction product $SiF_2(g)$. The $SiF_2(a)$ level is derived from measurements from temperature programmed desorption, whereas that of SiF(a) is derived from measurements from MMBRS (see text). For comparison, the binding energies implied by the corresponding bond dissociation energies for gas phase SiF_x species [69] are shown also.

energy of fluorine adatoms suggests that a pseudo-equilibrium between the adsorbed species is maintained in the MMBRS experiments.

Our examination of the kinetics of $SiF_4(g)$ formation is considerably less detailed than those conducted with respect to $SiF_2(g)$. Depending on the initial coverage of fluorine adatoms, $SiF_4(g)$ formation was observed over the temperature range of 120–800 K. We attempted a quantitative analysis of the two-peaked desorption feature occurring between 400 and 800 K. Both the shape (i.e., FWHM) and the shift of the peak temperature with increasing initial coverage for these two peaks suggested second-order kinetics. An analysis of the spectra by two independent methods gave kinetic parameters of $E_d = 32\text{–}45$ kcal mol^{-1} and $k_{d,1}^{(0)} = 5 \times 10^8\text{–}6 \times 10^{12}$ s^{-1} for the peak near 700 K, and $E_d = 17\text{–}23$ kcal mol^{-1} and $k_{d,1}^{(0)} = 2 \times 10^5\text{–}4 \times 10^7$ s^{-1} for the peak near 550 K. The discrepancy between the two methods of analysis is most probably associated with the assignment of a fixed reaction order and/or fixed kinetic parameters when fitting the entire peak shape. Comparison of these kinetic parameters to those found for the gas phase decomposition (i.e., pyrolysis) of $Si_2F_6(g)$ is useful. Specifically, Walsh and co-workers [70] have shown that $Si_2F_6(g)$ decomposes via a 1,2-fluorine shift to produce $SiF_2(g)$ and $SiF_4(g)$. The kinetics were found to be first-order, the parameters given by $E_d = 46.2 \pm 0.7$ kcal mol^{-1} and $k_d^{(0)} = 2.6 \times 10^{12 \pm 0.2}$ s^{-1}. These values are remarkably similar to those found for the 700 K desorption peak, i.e., where $E_d = 45 \pm 9$ kcal mol^{-1} and $k_{d,1}^{(0)} = 6 \times 10^{12 \pm 4}$ s^{-1}. A likely candidate for the mechanism of this reaction channel is $-SiF_x-SiF_3 \rightarrow -SiF_{x-1} + SiF_4(g)$, where

$x = 1, 2$. If, as Walsh and co-workers have suggested [70], the transition state for this 1,2-fluorine shift involves a three-center donor–acceptor complex, then the kinetics may be expected to vary depending upon if $x = 1$ or 2. This could explain the two-peaked desorption feature – i.e., one peak representing the reaction $\equiv SiF-SiF_3 \rightarrow \equiv Si + SiF_4(g)$, the other the reaction $-SiF_2-SiF_3 \rightarrow =SiF + SiF_4(g)$. In regards to possible future spectroscopic investigations we note that the two-peaked desorption feature can be "decoupled". That is, if one anneals adlayers representative of initial coverages of ≥ 5 ML to a tempera-ture of 625 K, thus desorbing the 550 K feature, cools the substrate to 120 or 300 K, and heats the substrate to 800 K, only the 700 K desorption feature appears. Specifically, there is no "mixing" of the two desorption features upon cooling the substrate to 300 K. Consequently, a spectroscopic investigation of the adlayer before and after a 625 K anneal could be useful in determining the reaction channels that lead to the production of $SiF_4(g)$.

The most important conclusion we can draw from our examination of the steady-state reaction of $F_2(g)$ with the Si(100) surface is that we can exclude any significant reaction occurring via an Eley–Rideal mechanism, i.e. $F_2(g)$ *must adsorb dissociatively for the reaction to occur*. Based on the sensitivity of our mass spectrometric detection, we place an upper limit on reaction via an Eley–Rideal mechanism of 10^{-2} of that measured and associated with a Langmuir–Hinshelwood mechanism. It is important to note, however, that under all conditions examined, the coverage of fluorine was always less than 1.5 ML, and the major reaction product was always $SiF_2(g)$. Thus, the possibility exists that the situation may be different at higher coverages.

It is of interest to compare our results to previous work by Mucha et al. [25], who examined the etching of Si by $F_2(g)$ for partial pressures of F_2 of 1–500 Torr and temperatures of 300–450 K. Summarizing, these workers found that the etch rate varied linearly with P_{F_2} for pressures below ~ 10 Torr, with the relative increase in the etch rate decreasing with P_{F_2} above 10 Torr. The etch rate (R_{etch}) was found to be described well by an Arrhenius expression, with an activation energy of 9.2 kcal mol^{-1}. At $P_{F_2} = 1.0$ Torr and $T = 455$ K, the measured etch rate was found to be 100–300 Å min^{-1}, which for Si(100) corresponds to 1.23–3.7 ML s^{-1}. Based on both the measured rate of reaction and the activation energy, our results from temperature pro-grammed decomposition (cf. figs. 6 and 7) imply that the coverage of fluorine under these "high" pressure conditions was 5 ML or greater. A useful quantity to derive from the results of Mucha et al. is the reaction probability of the F_2 molecules $\Re_{F_2}$. This quantify is defined as $\Re_{F_2} = 2R_{etch}/(F_{F_2}/n_s)$ where (F_{F_2}/n_s) is the impingement rate of the F_2 molecules. The factor of 2 arises from the assumption that SiF_4 is the major reaction product under these conditions. At $P_{F_2} = 1.0$ Torr and $T = 455$ K we find that the reaction probability is calculated to be $\Re_{F_2} = (0.63-1.9) \times 10^{-5}$. It is of interest to compare this value to our measured value for the probability of dissociative

adsorption. In particular, at $T_s = 120$ K and for coverages above 3 ML, we find from the data shown in fig. 1 that $S_{F_2} \simeq 10^{-3}$. Thus, if we equate the dissociative adsorption probability and the reaction probability, which is valid provided the fluorine adatoms produced do not recombine to form molecular fluorine and then desorb, the lower value calculated for the reaction probability is due to either the higher temperature, or the presumably higher coverage. Unfortunately, it is difficult to unambiguously resolve this issue since our data do not extend beyond 4 ML.

As stated above, Mucha et al. [25] observed that the relative increase in the etch rate decreased with increasing F_2 partial pressure. They attributed this to "Langmuir-like isotherm behavior". We have fit their data to a Langmuir isotherm representative of molecular *nondissociative* adsorption of F_2. That is, we assume that adsorption at high coverage proceeds through an extrinsic precursor state, and, under reaction conditions, the probability for dissociative adsorption is proportional to the coverage of F_2 molecules in this extrinsic precursor state. Moreover, we assume this probability to be much less than unity, which is justified both by our data for the adsorption kinetics at high coverage (cf. fig. 1) and by the above calculated reaction probabilities. Thus, a virtual equilibrium will be established between the gas phase F_2 molecules and the extrinsic precursor state, and we may apply the classical Langmuir isotherm [71], i.e., $R_{etch} \propto \theta_{F_2'} = K_{F_2'}(T)P_{F_2}/[1 + K_{F_2'}(T)P_{F_2}]$. The least-squares fit to the experimental data is shown in fig. 29. The temperature dependent equilibrium coefficient $[K_{F_2'}(T)]$ is found to be given by 9.3×10^{-6} Pa^{-1}. Employing a statistical mechanical formalism to calculate the preexponential factor of this coefficient we find that the implied heat of adsorption for the extrinsic precursor state is 6 kcal mol^{-1}. This value is well within the expectations for a weakly bound molecular adsorption state. Thus, the data of Mucha et al. [25] are entirely consistent with a reaction between adsorbed fluorine atoms and the Si substrate, with the dissociative adsorption of the F_2 molecules mediated by an extrinsic precursor state.

The importance of the extrinsic precursor state to the steady-state etching of Si by F_2 sheds some light on the feasibility of various methods that could be employed to enhance this reaction. Let us assume for the moment that the dissociative adsorption of F_2, at a constant substrate temperature, is only weakly dependent on coverage above 3 ML (cf. fig. 1). This is reasonable since the configuration of the *topmost* layer of the Si substrate, which presumably controls the adsorption kinetics, probably changes very little as the coverage increases beyond 3–5 ML. This implies that the reaction probability calculated at 455 K (i.e., $(0.63-1.9) \times 10^{-5}$) differs from our measured adsorption probability at 120 K (i.e., 10^{-3}) due primarily to the difference in temperature. In this case, the activation energy associated with dissociative chemisorption will be less than that for molecular desorption. Furthermore, with respect to the gas phase F_2 level, this suggests that the dissociative adsorption of F_2 at
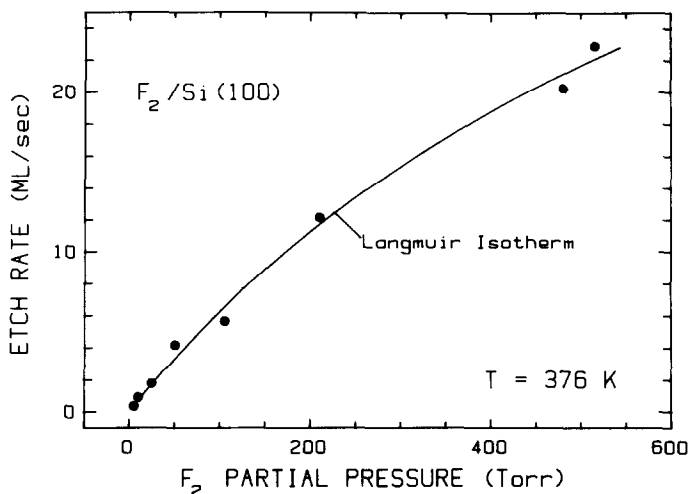
Fig. 29. Steady-state Si substrate etch rate at a temperature of 376 K as a function of the partial pressure of F_2 taken from the data of Mucha et al. [25]. The solid curve represents an analytic fit of the data to a Langmuir isotherm, where the etch rate is assumed to be equal to the rate of dissociative adsorption of F_2 and, hence, proportional to the coverage of F_2 in the extrinsic precursor state (see text).

high coverages *is not activated*. This conclusion is entirely consistent with the data displayed in fig. 1, where the average translational energy was found to have little effect on the adsorption kinetics. Thus, we suspect that efforts directed at enhancing the F_2 etching reaction of Si by increasing the average translational energy of the F_2 molecules will meet with little if any success.

5. Conclusions

We have examined in detail the interaction of fluorine with the Si(100) surface. The main conclusions of this work may be summarized as follows.

(1) F_2 adsorbs dissociatively on the clean Si(100) surface, and the initial (zero-coverage) probability of adsorption is equal to 0.46 ± 0.02. This value is independent of both substrate temperatures of $T_s = 120$–600 K, and the average translational energies of the incident F_2 molecules of $\langle E_{tr} \rangle = 1.5$–$19$ kcal mol^{-1}.

(2) There is an initial rapid phase of adsorption, which "saturates" at a coverage of $\theta_F \simeq 1.5$ ML, and corresponds to the attachment of fluorine atoms to the dangling bonds present on the Si surface atoms. For substrate temperatures of 300 K and above, this phase of adsorption is well characterized by second-order Langmuir kinetics. However, below 300 K, trapping into an

(molecular, mobile) extrinsic precursor state becomes important, which results in an adsorption probability that is nearly independent of coverage at 120 K.

(3) The adsorption of atomic fluorine is qualitatively distinct from molecular fluorine. Whereas the initial probabilities of adsorption are similar, above coverages of ~ 3–5 ML, the adsorption probability of F(g) exceeds that for F_2(g) by approximately two orders of magnitude. In addition, unlike molecular fluorine, the adsorption of atomic fluorine at high coverages may be activated.

(4) We found no evidence for an irreversible penetration of adsorbed fluorine adatoms into the Si substrate. The coverage range examined was representative of the monolayer regime.

(5) SiF_2(g) and SiF_4(g) are the only gas phase reaction products resulting from the thermal decomposition of silicon-fluoride adlayers, which are produced by exposing a clean Si(100) surface at 120 K to a beam of molecular and atomic fluorine. The relative yield of the two gas phase products depends strongly on the initial coverage of fluorine adatoms. For coverages below ~ 3 ML, SiF_2(g) is the major reaction product, whereas for coverages above 3 ML, the relative yield of SiF_2(g) remains constant while that of SiF_4(g) increases continuously. Independent of the initial concentration of fluorine adatoms, the thermal decomposition is terminated near 800 K by the removal of one monolayer of the Si substrate in the form of SiF_2(g).

(6) The kinetics of the desorption of SiF_2(a) depends in a complex fashion on the initial coverage of fluorine adatoms. A critical parameter is the ratio of the initial coverage to the apparent saturation coverage of the "fast" adsorption phase, which is $\simeq 1.2$–1.6 ML. In particular, the local coverage of fluorine adatoms in the vicinity of surface defects, where SiF_2(a) species are formed preferentially, influences the kinetics greatly. A manifestation of these effects is the observation of zero-order kinetics spanning the range of 1.0–0.3 ML for initial coverages of 1–1.3 ML. The kinetic parameters for this coverage regime, determined form two independent methods, are given by $E_d = 68$–86 kcal mol^{-1} for the activation energy and $k_{d,0}^{(0)} = 1.4 \times 10^{17}$–$1.4 \times 10^{22}$ ML s^{-1} for the zero-order preexponential factor. This reaction is limited by the rate of desorption of SiF_2(a).

(7) Examination of the adsorption kinetics of F_2 on a partially decomposed adlayer suggests that the thermal decomposition in the zero-order regime proceeds inhomogeneously, leaving separate domains where the local fluorine coverage is either near "saturation" or zero. Merely annealing an adlayer representative of the same coverage regime does not lead to adsorbate domain formation. Therefore, the major driving force for domain formation is associated with the decomposition reaction itself. We propose that the most likely scenario that can explain the inhomogeneity and zero-order behavior of the decomposition involves preferential reactivity at surface defects, such as atomic steps.

(8) In the limit of very low fluorine adatom coverages the decomposition

reaction that produces $SiF_2(g)$ is second-order in the coverage of fluorine. The kinetic parameters were found to be given by $E_d = 59$ kcal mol^{-1} for the activation energy and $k_{d,2}^{(0)} = 1.7 \times 10^3$ cm^2 s^{-1} for the second-order preexponential factor.

(9) The reaction channels that lead to the desorption of $SiF_4(g)$ between temperatures of 400 and 800 K are probably similar to the gas phase pyrolysis of Si_2F_6, which decomposes via a 1,2-fluorine shift to produce $SiF_2(g)$ and $SiF_4(g)$.

(10) The steady-state reaction between $F_2(g)$ and the Si(100) surface involves a reaction between chemisorbed fluorine adatoms, which result from the dissociative adsorption of F_2, and the Si substrate. In particular, we can discount any significant reaction occurring via direct reaction of gas phase F_2 and the Si surface atoms. Examination of "high" pressure kinetic data suggests that dissociative adsorption via an extrinsic precursor is important in the steady-state etching of Si by F_2 molecules.

Acknowledgement

References

[1] J.W. Coburn and H.F. Winters, Ann. Rev. Mater. Sci. 13 (1983) 91.
[2] D.L. Flamm and V.M. Donnelly, Plasma Chem. Plasma Proc. 1 (1981) 317.
[3] See, e.g., Proc. from the Workshop on W and other Refractory Metals for VLSI Applications, Vol. I/II, Ed. R.S. Blewer (MRS, Pittsburgh, PA, 1986).
[4] H.F. Winters and J.W. Coburn, Appl. Phys. Letters 34 (1979) 70.
[5] T.J. Chuang, J. Appl. Phys. 51 (1980) 2614.
[6] Y.Y. Tu, T.J. Chuang and H.F. Winters, Phys. Rev. B 23 (1981) 823.
[7] M.J. Vasile, J. Appl. Phys. 54 (1983) 6697.
[8] H.F. Winters and F.A. Houle, J. Appl. Phys. 54 (1983) 1218.
[9] D.E. Ibbotson, D.L. Flamm, J.A. Mucha and V.M. Donnelly, Appl. Phys. Letters 44 (1984) 1129.
[10] J.F. Morar, F.R. McFeely, N.D. Shinn, G. Landgren and F.J. Himpsel, Appl. Phys. Letters 45 (1984) 174;
F.R. McFeely, J.F. Morar, N.D. Shinn, G. Landgren and F.J. Himpsel, Phys. Rev. B 30 (1984) 764.
[11] N.D. Shinn, J.F. Morar and F.R. McFeely, J. Vacuum Sci. Technol. A 2 (1984) 1593.
[12] F.A. Houle, Chem. Phys. Letters 95 (1983) 5; J. Chem. Phys. 79 (1983) 4237; 80 (1984) 4851.
[13] M. Balooch, D.R. Olander and W.J. Siekhaus, Mater. Res. Soc. Symp. Proc. 38 (1985) 171.
[14] B. Roop, S. Joyce, J.C. Schultz, N.D. Shinn and J.I. Steinfeld, Appl. Phys. Letters 46 (1985) 1187.
[15] B. Roop, S. Joyce, J.C. Schultz and J.I. Steinfeld, Surface Sci. 173 (1986) 455.
[16] H.F. Winters and J.W. Coburn, J. Vacuum Sci. Technol. B 3 (1985) 1376.
[17] F.R. McFeely, J.F. Morar and F.J. Himpsel, Surface Sci. 165 (1986) 277.

[18] Y.A. Yarmoff and F.R. McFeely, Surface Sci. 184 (1987) 389.

[19] J.W. Coburn, H.F. Winters and T.J. Chuang, J. Appl. Phys. 48 (1977) 3532.

[20] T.J. Chuang, H.F. Winters and J.W. Coburn, Appl. Surface Sci. 2 (1979) 514.

[21] D. Thomson and C.R. Helms, Mater. Res. Soc. Symp. Proc. 38 (1985) 155.

[22] D.L. Flamm, V.M. Donnelly and J.A. Mucha, J. Appl. Phys. 52 (1981) 3633.

[23] M.J. Vasile and F.A. Stevie, J. Appl. Phys. 53 (1982) 3799.

[24] C.D. Stinespring and A. Freedman, Appl. Phys. Letters 48 (1986) 718;
C.D. Stinespring, A. Freedman, J.C. Wormhoudt and C.E. Kolb, Mater. Res. Soc. Symp. Proc. 68 (1986) 447.

[25] J.A. Mucha, V.M. Donnelly, D.L. Flamm and L.M. Webb, J. Phys. Chem. 85 (1981) 3529.

[26] J.A. Dagata, D.W. Squire, C.S. Dulcey, D.S.Y. Hsu and M.C. Lin, Chem. Phys. Letters 134 (1987) 151.

[27] M. Seel and P.S. Bagus, Phys. Rev. B 28 (1983) 2023; B 29 (1984) 1070;
P.S. Bagus, Mater. Res. Soc. Symp. Proc. 38 (1985) 179.

[28] K.J. Gruntz, L. Ley and R.L. Johnson, Phys. Rev. B 24 (1981) 2069.

[29] M.J. Bozack, M.J. Dresser, W.J. Choyke, P.A. Taylor and J.T. Yates, Jr., Surface Sci. 184 (1987) L332.

[30] T.M. Buck, in: Methods of Surface Analysis, Ed. A.W. Czanderna (Elsevier, Amsterdam, 1975);
W. Heiland and E. Taglauer, Methods Exptl. Phys. 22 (1985) 299.

[31] M.P. D'Evelyn and R.J. Madix, Surface Sci. Rept. 3 (1983) 413.

[32] J.A. Barker and D.J. Auerbach, Surface Sci. Rept. 4 (1985) 1.

[33] M. Balooch, M.J. Cardillo, D.R. Miller and R.E. Stickney, Surface Sci. 46 (1974) 358.

[34] D.J. Auerbach, H.E. Pfnür, C.T. Rettner, J.E. Schlaegel, J. Lee and R.J. Madix, J. Chem. Phys. 81 (1984) 2515.

[35] C.T. Rettner and H. Stein, J. Chem. Phys. 87 (1987) 770.

[36] S.G. Brass and G. Ehrlich, J. Chem. Phys 87 (1987) 4285.

[37] See, e.g., W.H. Weinberg, in: Kinetics of Interface Reactions, Eds. H.J. Kreuzer and M. Grunze (Springer, Heidelberg, 1987).

[38] J.R. Engstrom, M.M. Nelson and T. Engel, Phys. Rev. B 37 (1988) 6563.

[39] M.P. D'Evelyn, M.M. Nelson and T. Engel, Surface Sci. 186 (1987) 75.

[40] J.R. Engstrom and W.H. Weinberg, Rev. Sci. Instrum. 55 (1984) 404.

[41] S. Yamazaki, M. Taki and Y. Fujitani, Japan. J. Appl. Phys. 18 (1979) 2191.

[42] Leybold-Heraeus, unpublished results.

[43] M. Grunze, private communication.

[44] M.P. Seah and W.A. Dench, Surface Interface Anal. 1 (1979) 2.

[45] A. Cassuto and D.A. King, Surface Sci. 102 (1981) 388.

[46] D.A. King and M.G. Wells, Surface Sci. 29 (1971) 454.

[47] For an excellent discussion of the "beam reflectivity" method, see ref. [48].

[48] C.T. Rettner, L.A. DeLouise and D.J. Auerbach, J. Chem. Phys. 85 (1986) 1131.

[49] Even for the relatively "low" nozzle temperature of 965 K, a nozzle passivation procedure had to be adopted. Beginning at a temperature near 575 K and with F_2 gas behind the nozzle, the assembly was heated for one hour, the F_2 gas was evacuated, the temperature was raised 50 K to 625 K, and the assembly was heated in vacuo for two hours. Still holding the assembly temperature near 625 K, F_2 gas was placed behind the nozzle for one hour, the gas was evacuated, and the assembly was heated to 675 K for two hours. This procedure, heating in F_2 followed by heating in vacuo was repeated until the final in vacuo anneal at 925 K.

[50] P.W. Harland, S. Cradock and J.C. Thyne, Intern. J. Mass Spectrom. Ion Phys. 10 (1972/73) 169.

[51] R.J. Shul, T.R. Hayes, R.C. Weitzel, F.A. Baiocchi and R.S. Freund, J. Chem. Phys. 89 (1988) 4042.

[52] See, e.g., J.T. Yates, Jr., Methods Exptl. Phys. 22 (1985) 425.

[53] Note that a value for $\theta_\infty \simeq 4.0$ ML was employed to correct the coverages in a previous paper (ref. [38]).

[54] J.L. Taylor and W.H. Weinberg, J. Chem. Phys. 78 (1978) 259.

[55] T.S. Wittrig, D.E. Ibbotson and W.H. Weinberg, Appl. Surface Sci. 4 (1980) 234.

[56] R.H. Jones, D.R. Olander, W.J. Siekhaus and J.A. Schwarz, J. Vacuum Sci. Technol. 9 (1972) 1429.

[57] For a discussion of the limitations involved in applying MMBRS to the study of nonlinear reaction kinetics see, e.g., J.R. Engstrom and W.H. Weinberg, J. Chem. Phys. 87 (1987) 4211.

[58] W.T. Tysoe, N.D. Spencer and R.M. Lambert, Surface Sci. 120 (1982) 413.

[59] Previous work (ref. [58]) employed an analysis of the (considerably more complicated) response at the second harmonic frequency. However, once the assumption of second-order kinetics is made, there is no need to extend the analysis beyond the fundamental frequency, except for the purpose of verifying the assumption of second-order kinetics (cf. fig. 15). Since the signal-to-noise ratio is clearly greater at the fundamental, we have chosen this frequency for the quantitative aspects of the analysis.

[60] R. Opila and R. Gomer, Surface Sci. 112 (1981) 1.

[61] E. Taglauer, W. Heiland and J. Onsgaard, Nucl. Instr. Methods 168 (1980) 571.

[62] A.J. Schell-Sorokin and J.E. Demuth, Surface Sci. 157 (1985) 273.

[63] E.S. Hood, B.H. Toby and W.H. Weinberg, Phys. Rev. Letters 55 (1985) 2437.

[64] R.J. Hamers, R.M. Tromp and J.E. Demuth, Phys. Rev. B 34 (1986) 5343.

[65] W.H. Brown, D. Dollimore and A.K. Galwey, in: Comprehensive Chemical Kinetics, Vol. 22, Eds. C.H. Bamford and C.F.H. Tipper (Elsevier, Amsterdam, 1980).

[66] See, e.g., R.D. Shannon, Trans. Faraday Soc. 60 (1964) 1902.

[67] J. Kolaczkiewicz and E. Bauer, Surface Sci. 175 (1986) 508.

[68] W.H. Weinberg and J.T. Yates, Jr., private communication.

[69] R. Walsh, J. Chem. Soc. Faraday Trans. I, 79 (1983) 2233; Acc. Chem. Res. 14 (1981) 246.

[70] S.K. Bains, P.N. Noble and R. Walsh, J. Chem. Soc. Faraday Trans. II, 82 (1986) 837.

[71] A. Clark, The Theory of Adsorption and Catalysis (Academic Press, New York, 1970).